2013

Characterization Of Wave Propagation Through Composite Laminates

Chantly Smith
North Carolina Agricultural and Technical State University

Characterization of Wave Propagation through Composite Laminates

Chantly Smith

North Carolina A&T State University

A thesis submitted to the graduate faculty

in partial fulfillment of the requirements for the degree of

MASTER OF SCIENCE

Department: Mechanical Engineering

Major: Mechanical Engineering

Major Professor: Dr. Mannur Sundaresan

Greensboro, North Carolina

2013

The Graduate School
North Carolina Agricultural and Technical State University
This is to certify that the Master's Thesis of

Chantly Smith

has met the thesis requirements of
North Carolina Agricultural and Technical State University

Greensboro, North Carolina
2013

Approved by:

Dr. Mannur Sundaresan
Major Professor

Dr. John Kizito
Committee Member

Dr. Albert Esterline
Committee Member

Dr. Samuel Owusu-Ofori
Department Chair

Dr. Sanjiv Sarin
Dean, The Graduate School

Biographical Sketch

Chantly Smith was born on May 4, 1986 in San Diego, California. She received her Bachelor of Science degree in Mechanical Engineering from the Georgia Institute of Technology in Atlanta, Georgia in 2008. She was admitted to the Graduate Program in Mechanical Engineering at North Carolina A&T State University, Greensboro, North Carolina in 2012 where she is a candidate for a Master of Science degree. She has performed research on "Characterization of Wave Propagation through Composite Laminates."

Dedication

I would like to dedicate the work that I have done to my Moo Moo, who instilled in me at a very young age that education is an essential element for continued success.

Acknowledgements

I would like to thank my adviser, Dr. Mannur Sundaresan, for his guidance and support in conducting this research. Thanks to my committee for reviewing my work and offering up their expert knowledge and suggestions. Special thanks to Kassahun Asamene, Kumaran Gopal, Bonaventure Mills-Dadson, and the other members of the Intelligent Structures and Mechanisms (ISM) Lab, without which this work would not have been possible.

Table of Contents

List of Figures

List of Tables

Abstract

Structural Health Monitoring (SHM) seeks to develop systems for data collection, verification, and analysis to detect the potential for critical damage to occur in engineering structures. Composite panels are engineering structures that are susceptible to damages such as delamination and fiber breakage which greatly reduce the safety and performance of the structure. For composite materials that are widely used in aviation, early detection of such damage is important to prevent failure while the component is in flight. A common SHM method for damage assessment of composites is the Lamb wave propagation technique, whereby waves may be introduced into the composite panel via piezoelectric transducers. The propagating waves are measured after traveling through the region of interest to detect damage present in that region. Scanning laser vibrometry is a method often used to detect wave propagation patterns. The method is beneficial in that it is noncontact, nondestructive, and can be applied to virtually all geometries. Wave propagation patterns in composite panels are different from those seen in isotropic plates due to their anisotropy and the viscoelastic nature of the matrix materials. The use of a scanning laser vibrometer (SLV) to characterize wave propagation through a composite panel was explored in the present research. The characteristics of interest were the directionality of the propagating wave's amplitude, velocity, and attenuation. Thin lead-zirconate-titanate (PZT) actuators were bonded to an undamaged carbon/epoxy composite panel and pulsed to extract the wavefields using the SLV. Numerical simulations of the experiments were also performed to verify the results.

CHAPTER 1

Introduction

With the advent of complex engineering structures in civil, aerospace, and mechanical applications, so too has arisen the awareness in the need for damage prognosis systems. Such systems are beneficial in many ways, the most important of which is the safety of the individuals using the structure. Of concern to those responsible for the maintenance and care of the structure is the potential to shift from a timed-schedule approach to a status-based maintenance approach. In this way, labor, downtime, and costs associated with maintenance could be greatly reduced. Additionally, a system that is capable of effectively preventing the catastrophic failure of structures in operation would greatly increase the confidence level in such structures and result in much wider application.

1.1 Structural Health Monitoring

To satisfy the need for damage prognosis systems, Structural Health Monitoring (SHM) has been developed. SHM is the process of detecting and characterizing damage in engineering structures. A complete SHM system is capable of detecting, locating, classifying, and quantifying the severity of the damage. A network of embedded or bonded sensors is required to be affixed to the structure to acquire the data about the damage, while a central processor loaded with structural health criteria is necessary to assess the data in real-time. Either passive or active schemes of SHM may be employed, with the latter requiring actuators to excite the structure and the former relying only on the response of the structure to an applied load. An example of the passive approach is the acoustic emission (AE) technique, whereby elastic energy in the form of transient sound waves is spontaneously released by the structure as it undergoes deformation. For instance, a crack that is growing under tensile loading is able to be detected by the AE

technique; however, if the tensile load were below the threshold to grow the crack, the crack would go undetected. Unfortunately, in this way, only actively advancing defects are able to be detected. Another drawback is the need for high sensor densities on the structure in order to detect the AE signal. While the active scheme of SHM does require the use of actuators to excite the structure, this is not a drawback. In fact, the actuators provide the convenience of examining the structure within seconds at any location and anytime there is a need (Raghavan & Cesnik, 2007). The method selected for this research was the active scheme.

1.2 Composite Structures

One type of structure that has benefitted immensely from the advancements in SHM is composite materials. Structural composites are fiber and matrix layups comprised of two or more materials, such as carbon/epoxy or glass/epoxy/aluminum laminates. Laminates can be manufactured from fibers of various lengths, lamina of differing orientation, and layups of assorted stacking sequences. Advanced composites were developed to improve the overall mechanical and material properties of a structure, particularly the stiffness, strength, and density. For example, the high-stiffness, high-strength, and low-density characteristics of carbon/epoxy laminates make them ideal for aerospace and aircraft applications, where strong, lightweight materials are necessary. In addition, advanced composite materials are also valued for their long fatigue lives, adaptability to the intended function of the structure, and possibility to embed sensors for SHM during the manufacturing process (Daniel & Ishai, 2005).

Advanced composites, while desirable for their high performance characteristics, are susceptible to a slew of defects from a variety of mechanisms. For instance, if the fabrication process is not performed properly, abrasions, voids, resin-rich/resin-lean areas, fiber misalignments, and inclusions, among other defects, can result. While the composite structure is

in service, it is vulnerable to vibration, shock, scratches, dents, corrosion, foreign object impact, and even lightning damage in the case of aircraft panels. Each of these sources of damage is capable of causing one or more of the following defect types: de-bonds, delaminations, density variations, fiber breaks, matrix cracks, and/or wrinkles (Sierakowski & Chaturvedi, 1997).

It is apparent from the long list of damage sources and defect types that SHM is a useful tool for these types of structures. Not only is it necessary to utilize SHM to predict the behavior of such structures over the course of their service, but prior to installation it is practical and cost effective to perform inspections due to the potential for defects to occur during the materials production and fabrication processes or even the transport and storage of the structure. A nondestructive evaluation (NDE) method often employed to test material integrity prior to service is ultrasonic testing.

1.3 Ultrasonic Testing

Ultrasonic testing is a NDE technique which utilizes acoustic vibratory waves above the audible frequency range that are capable of detecting discontinuities in solid materials on both a macroscopic and microscopic scale. Ultrasound waves, typically higher than 20 kHz, introduced into a material impart high frequency mechanical vibrations that cause the material particles to oscillate as a result of the elastic nature of the material medium. The response of the material due to the vibratory excitation is as a direct result of the applied force. Forcing types in ultrasonic testing are dynamic loads, which can be classified as transient or steady state.

Ultrasonic testing techniques are primarily employed to determine the structural integrity of materials. Applications typically seek to detect discontinuities, measure the thickness of a structure, determine the elastic moduli of a material, study metallurgical structure, or evaluate the effect of processing variables on the component. An early example of ultrasonic testing

application is the examination of the first jet engine rotor forgings for internal discontinuities. The use of ultrasonic testing in these applications is possible due to the technique's high sensitivity which allows for detection of very small discontinuities, excellent penetrating power which permits examination of relatively thick sections, accuracy in measuring discontinuity position and size, speedy response which allows for rapid, even automated, testing, and necessity to have access to only one surface. These advantages make ultrasonic testing attractive for its versatility, sensitivity, directivity, and convenience. The limitations of ultrasonic testing are few and relate directly to properties of the structure, such as unfavorable geometry or undesirable internal structure.

The mechanical vibrations used in ultrasonic testing are transferred to a test structure by means of electromechanical transducers, which transform electrical energy into mechanical energy, and vice versa. Transducers are capable of generating longitudinal, shear, and surface waves by refraction and mode conversion. For this reason, in order to analyze results of ultrasonic testing, an adequate understanding of waves and wave propagation is necessary (Green, 1991).

1.4 Wave Propagation

A wave is a disturbance or oscillation that transfers energy through space and time. The phenomenon of wave propagation is the transmission or spreading of the localized disturbance in a medium to other parts of the medium. Wave propagation is characterized by a wave equation that depends on both position and time. While waves can propagate through many different types of media, of interest to this research is wave propagation in solids.

Wave propagation in solid media occurs in one of two ways: as bulk waves through an infinite or semi-infinite medium or as guided waves in the case of media with boundaries. Both

bulk and guided wave propagation are governed by the same set of partial differential equations, however, they are fundamentally different in a few ways. Being that bulk waves travel in the bulk of material, they also travel away from boundaries, which simplifies the mathematical solution of the governing equations since there are no boundary conditions to satisfy. By contrast, guided waves rely on boundaries for their existence, as is the case for surface waves and plate waves. It is this reliance that complicates the solution to a guided wave problem as boundary conditions must be addressed. Due to these complexities, some cases exist where an analytical solution to a guided wave problem is not even possible.

Another fundamental difference between bulk and guided waves is the number of modes that are present in the wave propagation problem. Bulk wave problems have a finite number of modes, primarily longitudinal (compressional), and transverse (shear horizontal or shear vertical). Guided wave problems generally have an infinite number of modes associated with them, such that a finite body could potentially support an infinite number of different guided wave modes (Rose, 1999).

1.5 Objective

The finite structure of a composite laminate transmits guided waves, and the complex nature of the guided wave problem due to the boundaries and multiple wave modes, as well as the anisotropy of the material, is explored in this research. The purpose of this research is to utilize the laser vibrometry technique for characterizing wave propagation through composite laminates. The characteristics of the wave propagation of interest are the directionality of the amplitude, velocity, and attenuation of the wave modes. Numerical simulations are performed to draw comparisons about the experimentally generated wave modes.

1.6 Thesis Structure

The information in this thesis work is structured as follows: Chapter 2 summarizes a literature review conducted to better understand wave propagation in a plate structure, as well as the current methods used for damage detection in composite materials. Chapter 3 describes the methods used to create the finite element model and the setup of the experiments performed. Chapter 4 displays the results and provides analysis for the simulation and experiments whose methodology was explained in the previous chapter. Chapter 5 contains a discussion of the work conducted and offers some suggestions for future research.

CHAPTER 2

Literature Review

Wave propagation in solid media has been studied extensively in the area of mechanics. The study has been led by pioneers including Rayleigh, Navier, Stokes, Poisson, Lamb, Love, Auld, and Achenbach. Ultrasonic wave propagation has become increasingly important in NDE, what with its many applications and the variety of available transmission and detection techniques. The literature reviewed for this research provides more information on wave propagation theory, methods of ultrasonic wave excitation and detection in composite structures, and signal processing and analysis options. Common ultrasonic test methods include pitch-catch, pulse-echo, through-transmission, and immersion testing, all of which employ Rayleigh and/or Lamb waves for signal analysis.

2.1 Lamb Waves

In NDE of plate structures, the types of waves most often investigated for damage detection are Lamb waves. Named for their discoverer, Horace Lamb, these waves are plane strain guided waves that propagate within the traction-free boundaries of a free plate having a thickness of at most a few wavelengths of the propagating wave. The free plate, illustrated in Figure 1, with its inherent traction-free boundaries at $x_3 = \pm d$, has the corresponding boundary condition

$$t_i = \sigma_{ji} n_j, \tag{1}$$

where, at the boundary, t is the traction, σ is the stress, n is the normal vector, and i and j are indices 1, 2, and 3 in Cartesian tensor notation. Coupled with the boundary condition of Equation 1, the free plate problem is governed by

$$(\lambda + \mu)\nabla\nabla \cdot \bar{u} + \mu\nabla^2\bar{u} = \rho\frac{\partial^2\bar{u}}{\partial t^2}, \tag{2}$$

which is the equation of motion in vector notation in the absence of body forces, where λ and μ are Lame's constants, ∇ is the gradient function, ∇^2 is the Laplacian function, $\bar{u} = (u_1, u_2, u_3)$ is the vector displacement, and ρ is the density of the material. Exact solutions to the free plate boundary value problem have been obtained using displacement potentials and partial wave techniques, each explained extensively in literature (Rose, 1999). Solution by the method of potentials is fairly simple, but is only useful for isotropic plates. The partial wave, or transverse resonance, technique is suitable for anisotropic plates, such as composite structures. The transvers resonance technique leads more directly to wave solutions and provides added insight into the physical nature of waves, which is lacking in the displacement potentials method.

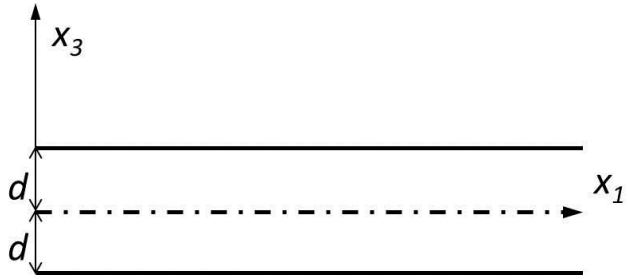

Figure 1. The free plate.

Lamb waves propagate as extensional waves such that the particle vibration contains a component that is perpendicular to the wave motion. The full motion of a particle in a traveling Lamb wave is elliptical and oscillatory in nature, leading to a time-variant trajectory (Neumann et al., 2012). Lamb wave particle motion gives rise to different modes, primarily symmetric (S_n) and antisymmetric (A_n) modes. The two basic modes in which Lamb waves occur are S_0 and A_0, pictured in Figure 2. These wave modes are dynamic properties that can change depending on the source of the signal, and can propagate independently of the other mode (Holford & Lark, 2005). The different modes are distinguished by observing the ratios of wavelength to thickness and frequency; these values are unique for each wave mode. The vibration patterns experienced

through the thickness of a plate during Lamb wave propagation differ for different Lamb wave modes, as well as differ for the same mode at different frequencies (Guo & Cawley, 1993).

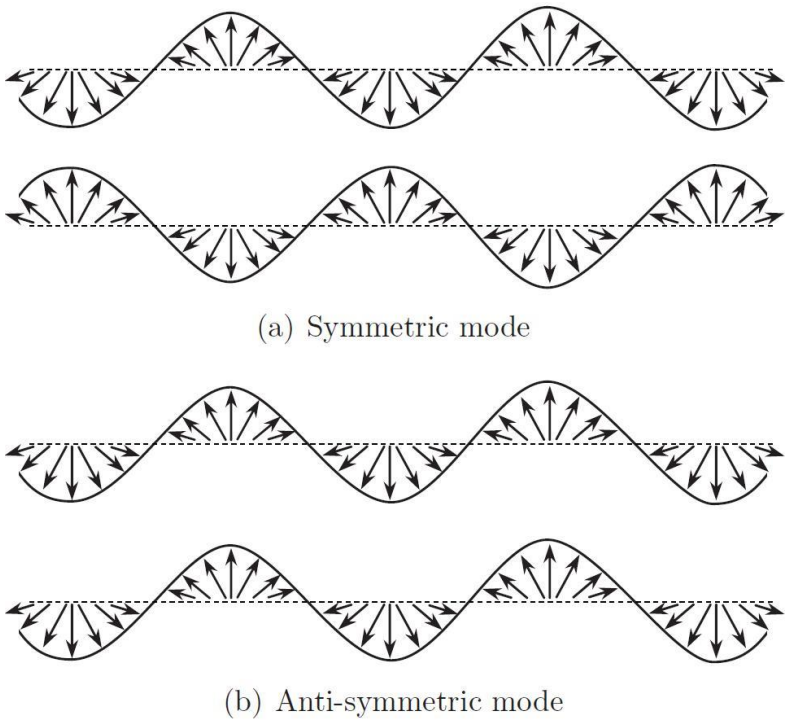

Figure 2. The basic Lamb wave modes (Holford & Lark, 2005).

Lamb waves contain both longitudinal and transverse waves which bounce between the two bounding surfaces as they travel along the length of the plate. When ultrasonic energy encounters the upper and lower surfaces, mode conversion takes place from longitudinal to transverse, and vice versa. Wave packets, or guided wave modes, occur in the plate after some time of propagation due to superposition of the waves. These guided wave modes develop at certain values of the acoustic frequency, *f*, and plate thickness and travel as a single wave with well-defined properties, such as wavelength and propagation velocity, in the plane of the plate. These individual waves have two velocities associated with them, group and phase velocity. The group velocity, c_g, termed "velocity of wave packets" by Heisenberg, is calculated from the time shift of the wave packet, or envelope, when the propagation path is changed (Rose, 1999). The

phase velocity, c_p, is the time shift between two similar phase features in the pulse, such as the peak of a pulse cycle when the propagation distance is changed. The equations of these velocities are represented by

$$c_p = f\lambda \tag{3}$$

and

$$c_g = c_p + f\frac{dc_p}{df}, \tag{4}$$

where λ in this case is the acoustic wavelength (Alers, 1991).

Lamb wave propagation depends on multiple factors, including density and elastic and material properties of the plate. Lamb waves are also highly dispersive, causing their propagation velocity to depend on the product *fd*, where *d* is the plate half-thickness (Giurgiutiu, 2005). As a result of these many dependencies, Lamb wave analysis can be very complex, especially if performed in a three-dimensional medium. As such, Lamb waves are often simplified to an idealized model by the plate wave approach. Within this approach, the fundamental modes, S_0 and A_0, are modeled as pressure and flexural plate waves, respectively. In this way, Lamb's theories are valid for relatively low frequencies (Neumann et al., 2012).

As the predominant waveforms introduced in industrial ultrasonic applications to composite materials are compressional and shear waves, Lamb waves are an obvious choice for detection. Additionally, Lamb waves are abundant since they are mathematically the normal modes of plate vibration. The features of Lamb waves that make them useful for SHM are their sensitivity to various damage types and the relatively long distances they are capable of traveling within a test structure. Due to these attractive qualities, Lamb waves have been analyzed extensively in the literature.

Among the first researchers to demonstrate the potential of Lamb wave methods for damage detection in composite materials were Guo and Cawley (1993). One of their studies concentrated on the numerical and experimental investigation of the S_0 mode in cross-ply laminates to quickly and reliably detect relatively large defects, such as 10- to 20-mm-diameter delaminations, through the thickness of the laminate. The S_0 mode was selected since it is capable of traversing distances of the order of 1 m in composite specimens, and as such, is useful in long-range nondestructive inspection. The pulse-echo method was used in which two transducers are employed, one of which is the transmitter of the Lamb wave and the other is the receiver. To determine if a defect was present, the S_0 mode reflections received by the receiving transducer were identified by their arrival time. For an undamaged specimen, the only reflections present were those from the edges of the plate. If a defect were present, additional reflections would be identifiable prior to the edge reflections. The limitations on the technique were found to be attenuation in the laminates and the signal-to-noise ratio of the transmitter-receiver system. Prior research found that good signals could be acquired for 10- to 20-mm-diameter delaminations at a transmitter-receiver distance of at least 500 mm.

Guo and Cawley also found that a very important characteristic in the interaction of Lamb waves with delaminations through the thickness of the laminate is the abrupt change in stiffness between adjacent layers of a cross-ply laminate. The abrupt change in stiffness is the cause of discontinuities in the shear stress distribution through the thickness of the plate, resulting in zero shear stress across certain lamina interfaces. At these levels of zero shear stress within the laminate, the wave propagated as it would in a free plate with no intermediate reflections emitted, even if a delamination were present. In some of the numerical simulation cases, where reflections from delaminations were able to be detected, the reflected waveform

appeared markedly different from the input waveform. The difference between the input and output waveforms was most likely partly due to some mode conversion from S_0 to A_0, which moves slower and is more dispersive, giving rise to spreading of the waveform. Another cause could be reflections generated at both ends of a small delamination relative to the spatial extent of the signal. Such reflections from relatively small delaminations tend to overlap, but can be easily resolved for longer delamination lengths.

Another characteristic investigated in the same study was the symmetry of the S_0 Lamb wave mode. The experimentally measured responses were found to be quite similar for delaminations equidistant from the top and bottom surfaces of the laminate, respectively, one being near and the other remote from the transducer. The similarity in response is true for specimen layups that are symmetrical with respect to the midplane. The symmetry of the S_0 Lamb wave mode also showed the sensitivity of the method to delaminations close to the excitation surface, as well as on the opposite side.

Many other studies have used piezoelectric transducers to verify the feasibility of using guided waves to detect defects in various configurations. Another such study used piezoelectric elements excited with short sinusoidal pulses on undamaged and damaged composite beams to study the ability to use Lamb waves for delamination detection at low *fd* products (Díaz-Valdés & Soutis, 2002). The arithmetic difference between the undamaged and damaged waveforms was taken to appreciate the changes seen from delaminations induced by progressively inserting a thin scalpel blade into the midplane of a quasi-isotropic composite beam. In the presence of damage, the first reflections from the boundary taken directly from the measurements were reduced in amplitude. The amplitude of the reflections from the boundary taken from the arithmetic difference increased with increasing delamination size, however. This phenomenon

was due to the fact that the time of travel of an A_0 Lamb wave is greater in a specimen with delaminations than an undamaged specimen, since the wave essentially travels through two regions of smaller thickness as it encounters a delamination. The time differences seen between the maximum peak of the input pulse and the maximum peak of the signal reflected from the boundary, as well as between the maximum peak of the input pulse and the maximum peak of the signal reflected from the delamination, were used to reasonably estimate the location of the delamination.

As there are presently no best known methods of using Lamb waves for damage detection, Kessler et al. (2001) attempted to optimize various parameters based on their sensitivity to damage detection. The parameters investigated experimentally and analytically included material properties and pulse frequency, amplitude, shape, and number of cycles. The speed of the propagating Lamb wave was related to the material properties of the specimen to determine the optimal design for the damage detection test. The thickness and the modulus were seen to have linear and square root relationships with the Lamb wave velocity, respectively, causing an increase in each property to have a corresponding proportional increase in the wave velocity. The density had the opposite relationship of the modulus, causing the wave velocity to slow proportional to an increase in density. Poisson's ratio was seen to have little to no effect on the wave velocity.

The pulse frequency was extracted from theoretically derived dispersion curves that related phase velocity to pulse frequency. From the dispersion curves it was able to be seen that fewer Lamb modes are excited at lower frequencies while more modes are present at higher frequencies. While the velocity is slower at lower frequencies, allowing for a more distinguishable received signal since there is more separation time, the dispersion curves at these

low values have steep slopes which denote a high sensitivity to small variations in frequency. The slope of the dispersion curve at higher frequencies is flatter, but the shorter wave pulse has the consequence of carrying more compressed information about the damage.

The investigation of the pulse amplitude performed by Kessler et al. revealed that while a higher amplitude led to a higher signal-to-noise ratio, the increase in applied voltage tended to drift the signal. Also, since an ideal SHM system should require little power to operate, a relatively low voltage of 5 V was chosen. The pulse shape investigation found that pure sinusoidal shapes excited Lamb wave harmonics the most efficiently, and a Hanning window that was approximated by a half-sine wave multiplied over the pulse width could be used to narrow the bandwidth to focus the maximum amount of energy into the desired actuating frequency.

One of the more complicated decisions Kessler et al. had to make for the Lamb wave techniques was found to be the number of cycles of the pulse used to actuate the piezopatches. A desirable narrow bandwidth with little dispersion could be achieved by a driving pulse with more periods. However, for a finite specimen, more periods in the pulse reduced the amount of time between the last sent signal and the first reflected signal, making the response difficult to interpret. The appropriate number of cycles was determined by taking the maximum number of waves that could be sent in the time it took for the lead wave to travel to the sensing piezopatch. For this study, half cycles were used to conveniently send symmetric, sinusoidal pulses into quasi-isotropic and sandwich beams.

The effect of damage size on the propagation of Lamb waves was investigated by Diamanti et al. (2007). The authors employed a linear array of transmitters placed along the width of the plate to propagate the first antisymmetric mode at low frequencies into quasi-

isotropic carbon-fiber-reinforced plastic laminates. The low frequency, 20 kHz, was selected as it reduces the resolution of the inspection and causes less attenuation. Critical defects of 20-25 mm diameter were created in the laminates by low-velocity impact and were successfully identified. The location of the damage along the length of the panel was successfully determined, though the extent of the damage along the width was not accurately predicted. In order to accurately predict the extent of the damage along the width, another array of transmitters would need to be imposed along the length direction.

2.2 Wave Amplitude Reduction

In a number of studies, including those performed by Guo & Cawley (1993) and Diamanti et al. (2007), attenuation and dispersion factors were taken into consideration during the experimental setup phase. These undesirable, yet inevitable, factors affect the propagating wave by reducing the amplitude over the distance of propagation. Other ways in which the amplitude of an ultrasonic waveform may be reduced are the reflection factor at an interface or boundary, beam spreading due to energy from the transducer spreading out during propagation, and even electronic processing, such as filtering and amplification (Rose, 1999).

2.2.1 Attenuation. In idealized materials, the strength of the signal amplitude is only reduced by the spreading of the propagating wave. However, all natural materials produce an effect which further weakens the signal in addition to the beam spread. This effect, called attenuation, is the combined result of scattering (reflections in directions other than the original propagation direction) and absorption (wave energy conversion to other forms of energy, such as heat). Ultrasonic attenuation is the rate of decay of the wave as it propagates through a material ("Attenuation of sound waves," 2013).

In general, for viscoelastic plate type structures such as composite materials, attenuation is due to absorption mechanisms, which include internal friction and internal scattering that are capable of reducing wave magnitudes. Attenuation by material absorption can be measured straightforwardly by imparting a single pulse into a material and measuring the amplitude of the received echo from the back surface of the sample (Adams, 2007). The received echo amplitude, A, is related to an initial, unattenuated amplitude, A_o, by

$$A = A_o e^{-\alpha z}, \tag{5}$$

where e is the exponential or Napier's constant, z is the distance from the initial location, and α is the attenuation coefficient. Equation 5 shows that the attenuation coefficient, and thus attenuation, is independent of density and wave velocity. The units of the attenuation coefficient are represented as loss of gain per distance, such as Nepers per meter (Np/m) or decibels per millimeter (dB/mm).

A profile of attenuation versus frequency can be created if measurements are taken at multiple frequencies for the same sample. The attenuation profile is characteristic of the particular material, as is the extracted attenuation coefficient at each frequency. Quoted values of attenuation are capable of giving only a rough indication of the actual attenuation since attenuation is highly dependent on the way the material was manufactured. Thus, more reliable and distinctive values of attenuation are generally obtained by experimental measurements of the particular material being used.

2.2.2 Dispersion. When the velocity of a propagating wave is dependent on its frequency or wavelength, the wave is exhibiting dispersion. The medium through which the dispersion occurs is a so-called dispersive medium. A dispersive wave is seen to "spread out" as it propagates through a dispersive medium.

Dispersion is also due to geometric effects that are a summation of reflection factor effects. The reflections at the top and bottom surfaces of a plate that produce guided waves inherently have dispersion effects. Dispersion relations between frequency and velocity of Lamb waves are commonly studied. One such study (Wang & Yuan, 2007), formulated the exact dispersion relations of the symmetric and antisymmetric wave modes in a composite laminate with arbitrary stacking sequence by the three-dimensional elasticity theory. Displacement and stress continuity conditions were imposed along the midplane of a symmetric laminate to decouple the symmetric and antisymmetric wave modes. From the dispersion relations, dispersion curves of Lamb waves of two types of composite laminates were numerically developed, which plotted dimensionless velocity c_p/c_T and c_g/c_T against dimensionless frequency $\omega h/c_T$, where $c_T = \sqrt{G_{12}/\rho}$ is the transverse wave velocity, ω is the angular frequency, and h is the full plate thickness. Experiments using PZTs to excite pure symmetric then pure antisymmetric modes in the composite laminates effectively modeled the dispersive and anisotropic behavior of Lamb waves.

From Wang and Yuan's dispersion curves, characteristics of the modes were extracted. The fundamental modes were the only Lamb modes that did not have a cutoff frequency. In the symmetric angle-ply laminate, for phase velocity, the S_0 mode exhibited low dispersion below frequency $\omega h/c_T = 0.5$, so at these values the wave packet is capable of retaining its shape as it travels since the different frequency components propagate at nearly the same velocity. Similarly, for the quasi-isotropic laminate, S_0 had little dispersion below frequency $\omega h/c_T = 1.25$. However, for the group velocity dispersion curves and for both angle-ply and quasi-isotropic laminates, the S_0 mode was seen to be highly dispersive. Contrarily, the A_0 mode exhibited little dispersion in both laminates beyond $\omega h/c_T = 1$.

As low dispersion is a desirable characteristic for many SHM applications, the selection of the diagnostic wave mode used is often based on the dispersive behavior. It is clear from the above that for lower frequency applications, the S_0 mode is favored over the A_0 mode, and vice versa. In addition to low dispersion, minimal attenuation and high sensitivity are valued for delamination detection. As the S_0 mode exhibits these characteristics, it is often used for such applications. Unfortunately, it can be difficult to experimentally excite the S_0 mode, since its amplitude is relatively weak compared to the A_0 mode when both are excited simultaneously. For this reason, some researchers, such as Díaz-Valdés and Soutis (2002), have opted to use the A_0 mode. Another favorable characteristic of the A_0 mode is its high resolution as it always has a much shorter wavelength compared to the S_0 mode.

CHAPTER 3

Methodology

3.1 Finite Element Modeling

In parallel to the experiments performed, Lamb wave generation was performed in finite element modeling. Comparisons between the experimental and finite element model will be drawn in the next chapter.

3.1.1 Material modeling. Composite materials exhibit complex behavior that needs to be appropriately modeled. Several approaches have been suggested in the literature, including the use of shell elements, as well as solid elements. The approach utilized for this research was a simplified representation of a cross-ply laminate that was symmetric about the midplane. Rather than modeling all 12 plies of the laminate that would be used in experiments, only 4 plies were modeled such that a stacking sequence of [0/90/90/0] resulted, with the 0° direction along the *x*-axis. Modeling in this way allowed for computation time savings without loss of information through the thickness. The quarter symmetry of the plate was exploited for the numerical model as it was for the experiment to further reduce computation time.

The quarter symmetric model was created in PreSys™ (PreSys™, 2010) with each ply having dimensions of 250 mm × 250 mm. The four plies were modeled in such a way that the bottom ply was coincident with the x-y plane and the *z*-axis was normal to the center point. The uniform mesh imposed on the laminate had solid elements with dimensions of 0.5 × 0.5 mm and a depth the same thickness as the individual ply. The top and bottom surface of each coincident ply was merged with the other plies for continuity. An isometric view of the modeled laminate is shown in Figure 3.

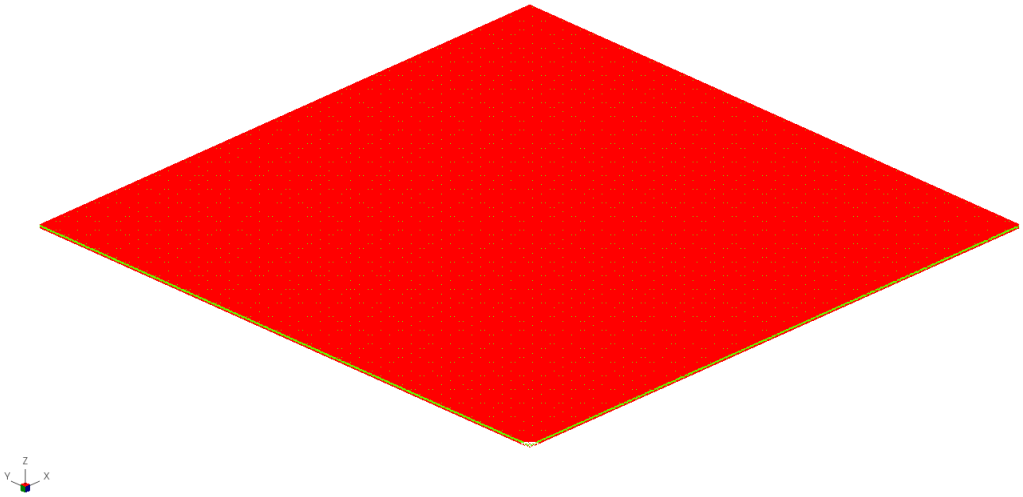

Figure 3. Cross-ply laminate modeled in PreSys™.

Laminate properties were taken from a finite element modeling reference book (Barbero, 2008) for unidirectional carbon/epoxy composites. The properties input for the 0° plies are listed in Table 1. The properties for the 90° oriented plies are the same, but with the property along the *x*-direction becoming the property along the *y*-direction.

Table 1

Laminate Properties Used in the Finite Element Model

Property	Symbol	Value
Elastic Modulus (GPa)	E_x	133.86
	E_y	7.706
	E_z	7.706
Shear Modulus (GPa)	G_{xy}	4.306
	G_{yz}	2.76
	G_{xz}	4.306
Poisson's Ratio	υ_{xy}	0.301
	υ_{yz}	0.396
	υ_{xz}	0.301
Density (g/cm^3)	ρ	1.52

3.1.2 Excitation modeling. Some researchers have attempted to model the actuating PZT as a "dummy" (Carrara & Ruzzene, 2013) while others apply forces and bending moments to the nodes to achieve the desired excitation (Yang et al., 2006; Díaz-Valdés & Soutis, 2002). For the numerical simulation performed for this research, forces were applied over a 9 × 9 element grid in the corner of the model to represent the pseudo-circular, central actuation of a PZT or, as is the case in Figure 4, PZTs. The forces applied along the edges were of the same magnitude, while the forces on the inset were resolved to act diagonal to the node. As will be explained in the next section for the experimental setup, dual-PZT excitation was used to excite either pure S_0 (both sides with positive direction forces) or pure A_0 (one side with positive forces, one side with negative forces) modes. In order to excite both modes at once, only one positive PZT excitation was included in a particular model.

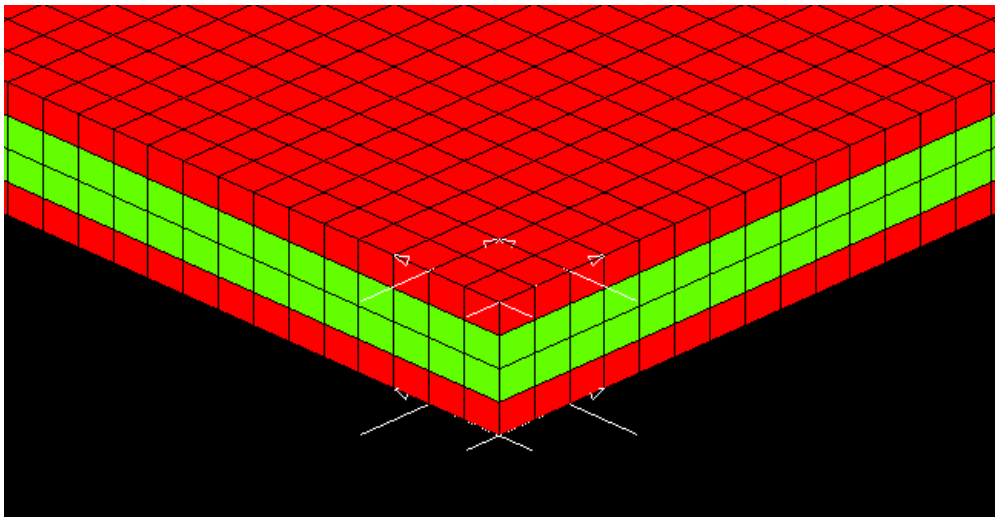

Figure 4. Forces applied on the cross-ply laminate model.

3.2 Experimental Setup

The experiment performed was excitation of a cross-ply composite laminate extract the characteristics of the propagating wave. The resulting wave propagation was captured using a scanning laser vibrometer.

3.2.1 Material selection. The material made available for this experiment was a cross-ply carbon-fiber-reinforced polymer (CFRP) laminate fabricated at the NASA Dryden Flight Research Center. The CFRP laminate, shown in Figure 5, was selected for its numerous aerospace applications. The laminate was comprised of 12 plies with a stacking sequence of $[0/90]_{3s}$ and a total thickness of 2.07 mm. Additional properties of the panel were a length of 609.6 mm, a width of 304.8 mm, and an ultimate stress of 965.3 MPa. To ensure no critical defects were present within the laminate, thermography was performed using a FLIR SC5000-Series thermography camera. Images taken, shown in Figure 6, show no signs of significant damage.

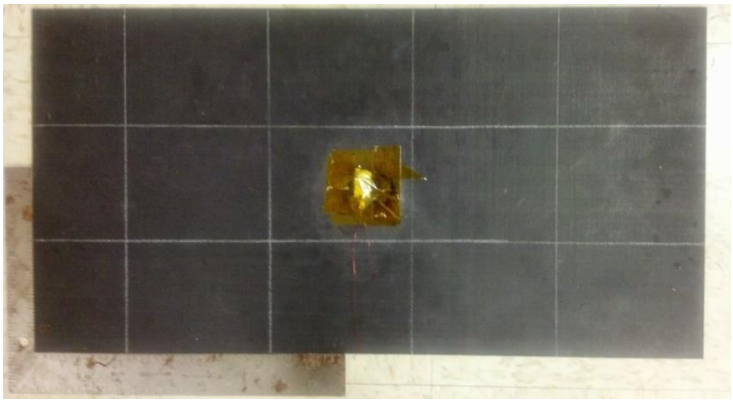

Figure 5. The CFRP laminate.

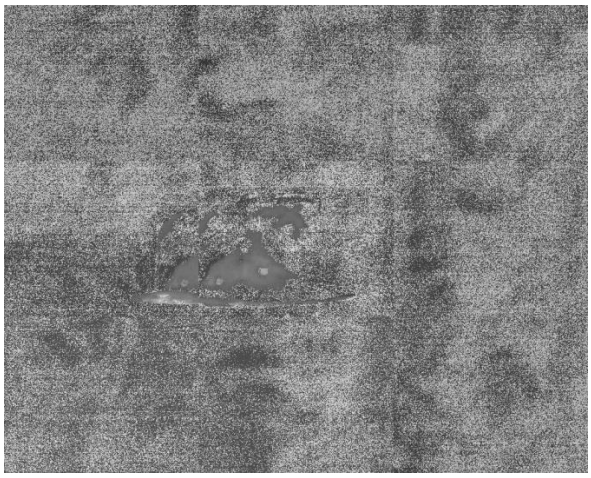

Figure 6. Thermographic image of the CFRP laminate, free of defects.

3.2.2 Excitation. In order to generate stress waves within the composite panel, an excitation had to be imposed. The selected excitation was the 5-cycle sine-Gaussian pulse seen in Figure 7. The pulse was imparted on a lead zirconium titanate (PZT) piezoelectric transducer (Piezo Systems) bonded to the surface of the panel. Due to the high frequency (200-500 kHz) excitation used in the experiments, a relatively thin PZT wafer was necessary ("Piezoelectric transducers," 2013). Preliminary testing conducted on an aluminum plate showed that the thinner the PZT wafer, the higher the amplitude of the S_0 mode response. As improved excitation of the S_0 mode was a secondary function of this research, a thinner PZT wafer was selected. Due to the fragility of the PZT wafer of 0.25 mm thickness, a PZT wafer of 0.51 mm was chosen.

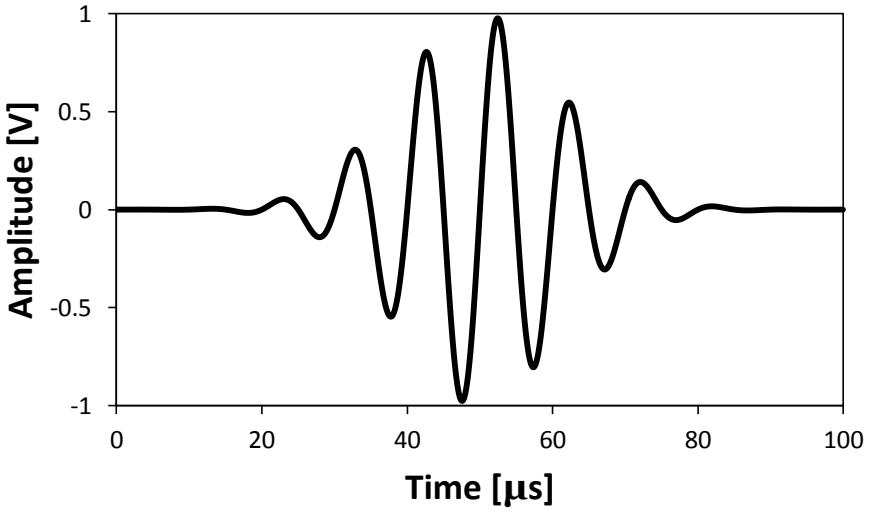

Figure 7. Sine-Gaussian pulse at 100 kHz.

In order to further improve the excitation of the S_0 mode, additional tests were performed on a 609 mm × 609 mm × 3 mm aluminum plate. This particular aluminum plate was chosen as the medium for the tests because results could easily be validated with past research conducted in the lab. Since symmetric modes of wave propagation move in symmetric fashion about the mid-

plane of the plate ("Modes of sound," 2013), it is understood that symmetric excitation from two sources of the same polarity on opposite sides of a panel would give rise to higher amplitude S_0 modes than a single source could. The reverse is true for A_0 excitation, such that sources of opposite polarity are required for higher amplitude signals (Su & Ye, 2004). These excitation phenomena are depicted in Figure 8. To determine the efficacy of this setup, two square PZT transducers, formed by cutting a rectangular 10 mm × 20 mm × 0.51 mm wafer in half, were bonded face up to the same position on each side of the aluminum plate. The resulting waveforms were acquired using an ultrasonic transducer affixed to the plate using permanent double-sided tape at a distance of 6 in away from the PZTs. The receiver distance of 6 in from the source was found in past research done on the aluminum plate to be the minimum required for discernible separation of the S_0 and A_0 modes in the AE waveforms. Additional tape was used to secure the ultrasonic transducer to the plate and create constant, uniform pressure.

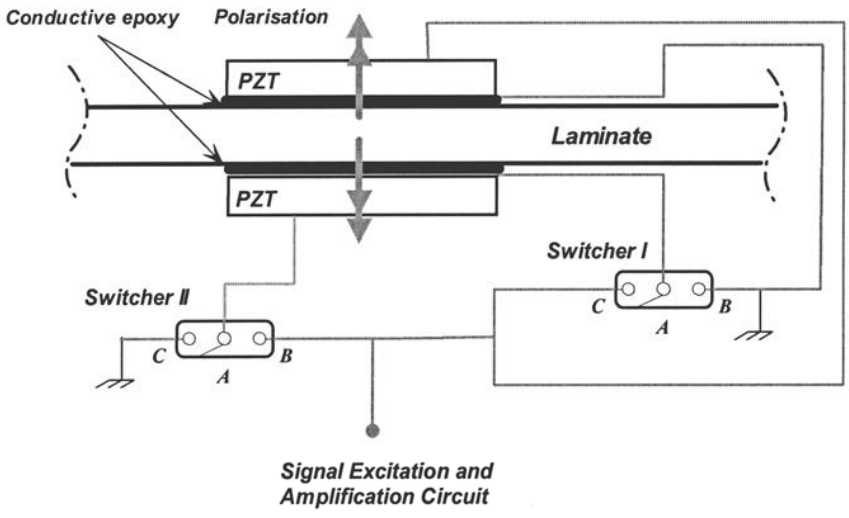

Figure 8. Dual-PZT excitation diagram (Su & Ye, 2004).

The full setup of the thick aluminum plate experiment is shown in Figure 9. A function generator (HP33120A, 15-MHz) loaded with a 19 V, 5-cycle sine-Gaussian wave was simultaneously input to both PZTs in order to actuate the plate. As mentioned before, the response of the plate was received by the ultrasonic transducer. The resulting waveforms were able to be viewed on an oscilloscope (LeCroy 9304CM, 200 MHz) by amplification of the ultrasonic transducer signal with a 34 dB gain preamplifier (Olympus Model 5682). The experiment was repeated for frequencies ranging from 200-500 kHz in increments of 50 kHz.

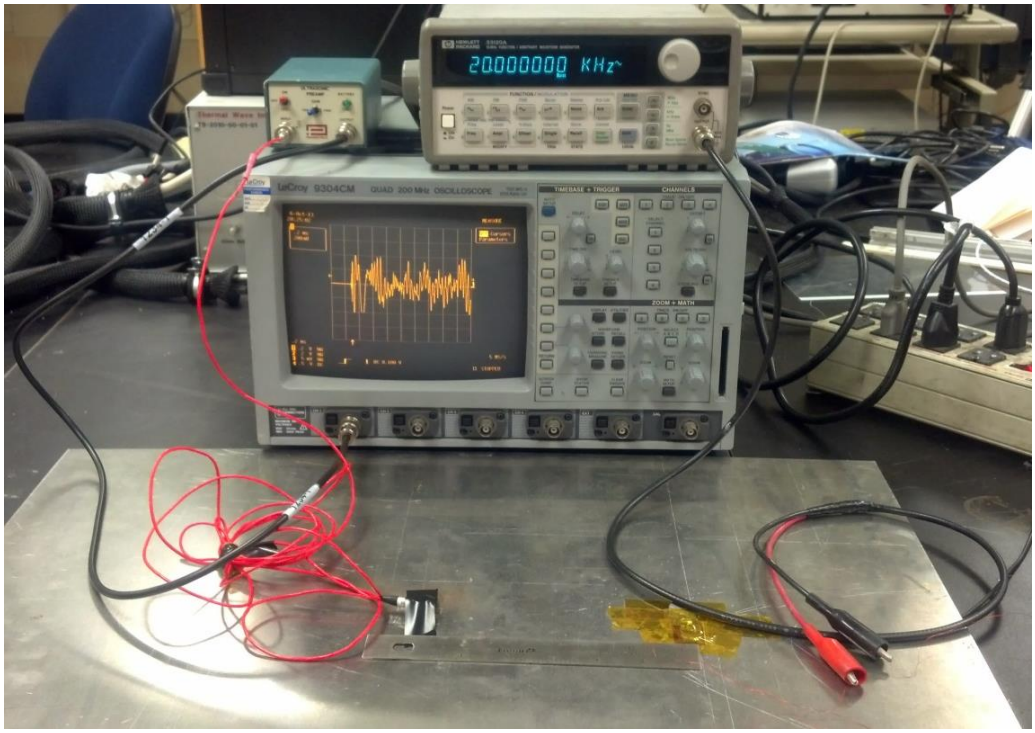

Figure 9. Complete setup for the aluminum plate test.

The composite panel was also excited by two PZTs, each bonded at the center of either side of the panel. Lamb waves tend to propagate parallel to each edge of the actuator, or circumferentially in the case of a circular excitation (Kessler et al., 2001). Since only the rectangular PZT transducers were readily available for experimentation, though circular excitation was desired, two octagonal transducers had to be fashioned from a single 9.96 mm ×

20.06 mm × 0.51 mm rectangular PZT wafer to impose a pseudo-circular excitation. As with the aluminum plate, the function generator was loaded with a 5-cycle sine-Gaussian wave, however, the voltage was lowered considerably to 0.8 V to accommodate input into a 300 dB power amplifier with a maximum input of 1 V (ENI 2100L RF). The amplification used was sufficient for the out-of-plane displacement wavefields to be sensed by a scanning laser vibrometer (SLV). Results of these experiments are presented in the succeeding chapter.

3.2.3 Data collection apparatus. The SLV used in the composite panel experimentation was a Polytec Scanning Vibrometer (PSV) system comprised of a scanning head with a Helium Neon (HeNe) laser (model OFV-055), a video control box (model OFV-310), a scanning vibrometer controller (model OFV-3001-S) and a personal computer with scanning software. The PSV system, shown in Figure 10, is a highly specialized instrument that is applied for the detection and analysis of vibrations emitted by surfaces. The technical specifications of the system, provided by Polytec (Polytec Manual), are given in Table 2.

Figure 10. A Polytec Scanning Vibrometer system.

Table 2

PSV Manual Technical Specifications

Scanning Vibrometer Head	
Angular Resolution	0.01°
Scanning Vibrometer Controller	
Range (mm/s/V)	Resolution (μm/s)
1	0.3
5	0.3
10	0.5
25	2
125	5
1000	10
A/D Converter	
Resolution	14 bits
Video Processing	
Resolution	720 × 480

The PSV system uses the principles of laser Doppler vibrometry (LDV) to acquire the wavefields. LDV applies the optical Doppler effect to coherent laser light reflected from a test surface to determine its magnitude and frequency content. The laser beam is focused on the object surface by means of mirrors, and the object surface scatters or reflects the light back to the laser source via a quarter-wave plate. From the backscattered light, the Doppler frequency shift, or phase shift, is demodulated by splitting the beam into reference and object beams. The beams are recombined at the interferometer that is fixed to the light source, where the shift of the object beam frequency imposes a beat on a photodetector. The measured beat frequency is directly proportional to the relative velocity between the object and light source, however, information about the sign (whether the object is moving toward or away from the light source) is not available. In order to overcome this limitation, heterodyne LDV incorporates an acousto-optic modulator, typically a Bragg cell, to shift the frequency of the reference beam and determine the sign of the velocity component parallel to the axis of the laser beam. The measured velocity is transformed to voltage by means of a digital decoder, which digitizes and processes the result as

a vibrometer signal (Johansmann et al., 2005). Figure 11 shows a schematic of the process just described.

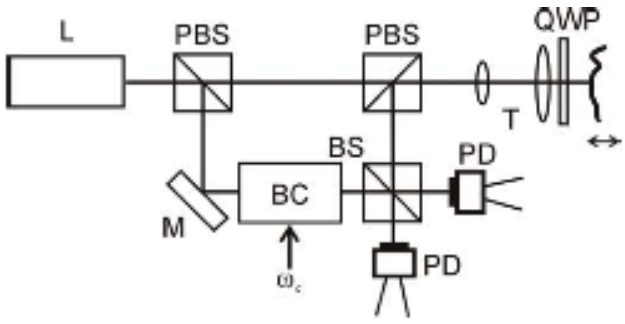

L=laser, PBS=polarizing beam splitter, QWP=quarter wave plate, M=mirror, BC=Bragg cell, PD=photodector, ω_c=BC reference frequency

Figure 11. Schematic of a SLV (Johansmann et al., 2005).

Most commercial SLVs are heterodyne, as is the case of the PSV system. An SLV performs the measurements based on the LDV principles described above at multiple points on the object surface defined by a scan grid by fine adjustments of the angle of the laser emitted from a scanning laser head utilizing control from an internal galvanometer. The measurements are repeated with unchanged parameters, and when combined, provide a video-like representation of time domain data. The type of excitation used to stimulate the measurement object determines the measurement parameter. The different types of excitation include periodic (repeating signal such as a sinusoidal vibration), transient (impulse such as a Gaussian pulse), and stochastic (random with noise such as a noise generator). For the study of Lamb waves, transient excitation provides useful information since the direction of the velocity vector is not constant but varies with time. In transient excitation, a pulse is generated on the object by a signal generator for each scanning point, causing a vibration that can be measured and analyzed by the SLV. For this experimentation, as was stated in section 3.1.2 and is depicted in Figure 7,

the transient sine-Gaussian pulse was utilized from an amplified signal from a function generator and the wavefields were detected by the SLV in the time domain. The schematic of the complete setup used in the SLV experiments, which is similar to the setup used by Pai (2007), is shown in Figure 12 with an image taken of an actual scan in progress provided in Figure 13.

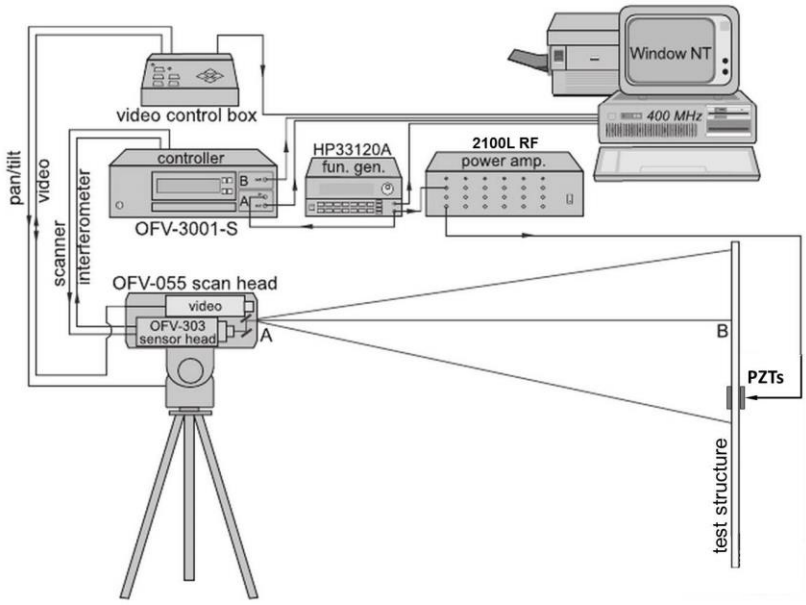

Figure 12. Complete setup for the SLV experimentation.

Figure 13. Actual SLV scan in progress.

The wavefields gathered from the PSV were to be used to determine the attenuation and velocity of the propagating wave through the cross-ply laminate along every direction incremented by 15°. Due to the symmetry of the laminate, a scan area was able to be selected over one-quarter of the plate. The reduced area effectively cut down scan time while still providing full-field information about the laminate. The scan grid had to be further reduced to eliminate points in the vicinity, or within 1 in, of each boundary to ignore points containing immediate reflections. As the laminate was twice as long as it was wide, more points could be taken at directions closer to the 0° direction than those directions closer to 90°. The scan grid had a resolution of 1 mm along each direction, and is shown imposed on the composite laminate in Figure 14.

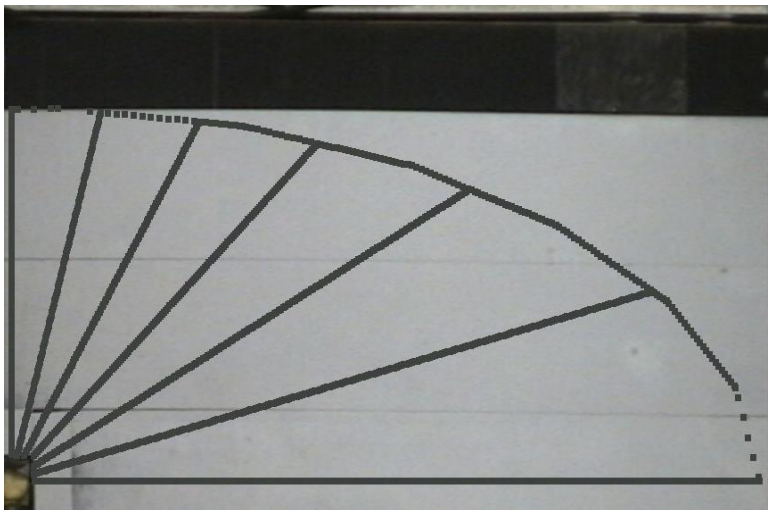

Figure 14. 127 mm × 279 mm radial scan grid.

3.2.3.1 Random noise reduction. In order for the SLV to receive accurate displacement information from the vibrating plate, various random noise sources had to be reduced. One such noise source, speckle, occurs when the optical sensor is subjected to elevated levels of inherent fluctuations in the laser light intensity backscattered from the surface. In an effort to diminish the speckle effect and account for differing surface qualities and/or surfaces with varying

distances for different measurement points, which create undesirably dissimilar noise levels, the PSV system employs several methods to reduce noise. Of these system methods, complex averaging of the signals was selected in the system settings in order to take a specified number of measurements of the same scan point and average them to reduce the effect of random noise. For measurements in this research, signals were averaged 15 times. The Tracking Filter setting, which uses the phase-locked loop principle to bypass intermittences in the backscattered laser light caused by the speckle effect, was used to reduce noise in the upper measurement range selected of 25 mm/s/V. Additionally, a band-pass filter was used on both the vibrometer and reference signals (Polytec Manual).

3.2.3.2 Systematic error reduction. The vibrometer signal level is affected by several controllable variables such as the laser beam focus, distance and angle between the front panel of the scanning head and the measurement object, and even the surface finish of the measurement object. These variables are capable of imparting systematic errors on the signal. Optimization of the instrument setup and measurement settings was performed in this research to reduce these error sources. Prior to each test, the system was allowed to warm up for 15 minutes to allow the HeNe laser the time required to reach optimum stability. The laser beam was focused with special care to ensure minimal external light interference so that the maximum possible intensity of the laser could be achieved. The distance between the scanning head and the measurement object of approximately 1650 mm was set to coincide with a maximum of the laser intensity, which occurs at $(231 + 205n)$ mm away from the front panel of the scanning head, with $n = 1, 2, 3\ldots$ Also, placement at this distance ensured that the laser beam did not hit the lateral points of the measurement area diagonally, further reducing the intrinsic error of using a one-dimensional SLV.

This research uses a SLV to measure Lamb waves. As mentioned in Chapter 2, Lamb waves travel in an elliptical, oscillatory manner. Since a one-dimensional SLV is only capable of measuring the velocity component parallel to the laser beam, much information about the propagating Lamb wave is lost. Though few data points in the scanning grid are precisely positioned along the axis of the laser beam that can possibly contain all of the information about the velocity of the vibrating object surface, the systematic error due to the use of the one-dimensional SLV was still able to be reduced by positioning the scanning head such that its longitudinal axis was perpendicular to the measurement area.

Since speckle noise depends on the ratio of the laser wavelength to the structural surface roughness (Pai, 2007), the surface of the composite panel had to be treated to contain the necessary reflective qualities for the laser. Given that evenly matte surfaces are ideal as opposed to highly reflective or transparent surfaces that do not allow much laser light to scatter back to the scanning head, several surface finishes were tried to determine a proper surface treatment. A reflective tape initially used was found to be too shiny and did not reflect enough laser light back to the scanning head, resulting in weak signal levels and a low signal-to-noise ratio. Retroreflective glass beads supplied by Polytec (P-RETRO-xxx) possessed the appropriate properties such as a high index of refraction for strong laser signals, but gave rise to other issues. Difficulty in spreading the microspheres uniformly as well as individual vibrations of the spheres led to wavefields with elevated degrees of error. Ultimately, a retroreflective tape manufactured by 3M (Scotchlite™ High Gain Reflective Sheeting 7610) was selected as it provided the ideal, uniform, matte surface with a high gain that reflected the most laser light back to the scanning head.

CHAPTER 4

Results

4.1 Numerical Simulation

The numerical simulation was performed for three cases: dual-PZT symmetric excitation, dual-PZT antisymmetric excitation, and single PZT excitation. Two nodal displacement waveforms in the *z*-direction were selected to determine the group velocity of the propagating wave in each dual-PZT excitation case. Due to the large difference between the absolute values of the S_0 and A_0 mode amplitudes, the *z*-displacements could not be properly displayed for the single-PZT excitation case. To compensate, the *x*-stress was selected to be displayed, as the amplitudes provided were comparable. This compensation is also possible due to the fact that Lamb waves have components in all directions and may be recognized by displacement and stress distributions. All nodes and elements were selected along the 0° direction.

Figure 15 shows the normalized displacement waveforms for the dual-PZT symmetric excitation. The S_0 wave packets for the two nodes are present with peaks at 21.7 and 26.5 μs. The distance between the selected nodes was 32 mm. Due to the finite nature of the modeled plate and the high speed of the travelling wave, reflections may be seen after 70 μs. The results from the dual-PZT antisymmetric excitation are shown in Figure 16. The A_0 wave packets occur with peaks at 44 and 72 μs, with the distance between the selected nodes being 42.5 mm. Since the speed of the A_0 mode is much slower than the S_0 mode, reflections are not visible in the 200 μs time allotted for the simulation. Given sufficient time, reflections could have been generated as they were for the dual-PZT symmetric case.

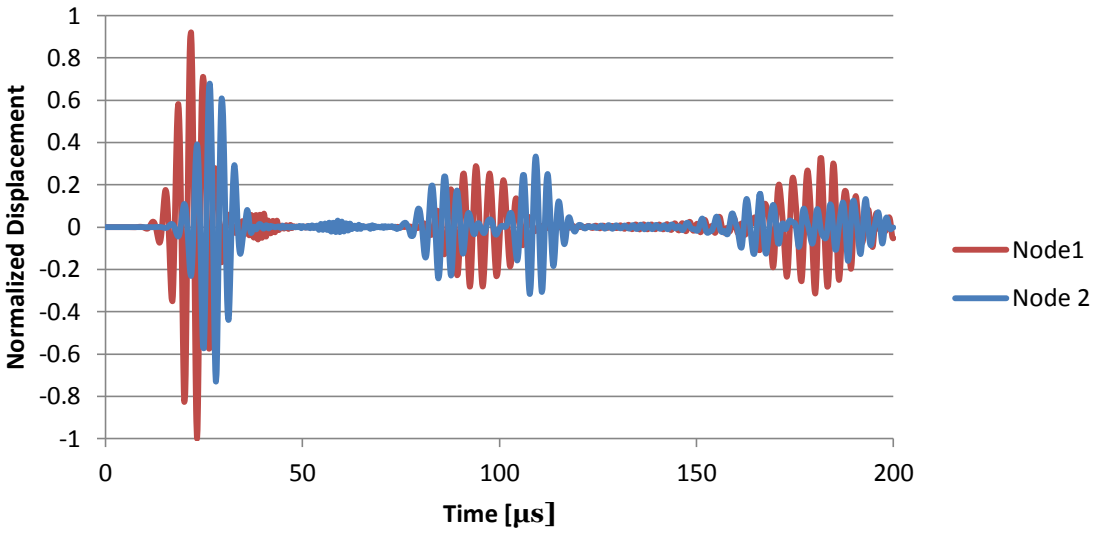

Figure 15. Numerical simulation symmetric excitation, *z*-displacement.

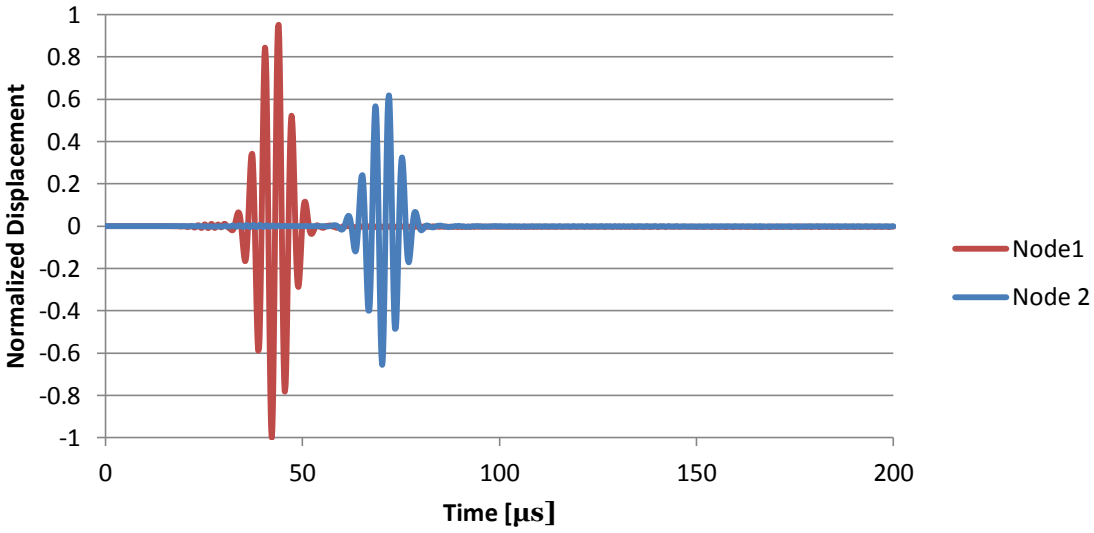

Figure 16. Numerical simulation antisymmetric excitation, *z*-displacement.

The single-PZT excitation simulation resulted in the presence of S_0 and A_0 mode wave packets in the waveforms shown in Figure 17. The slower speed of the A_0 mode is clearly seen as the difference in time between the S_0 and A_0 wave packets for Element 1 is 28 µs and for Element 2 is 49.3 µs. The distance between the selected elements was 41.5 mm. The speeds for

each case were calculated by dividing the distance between the nodes or elements by the time shift between the respective wave packets of each waveform. The calculated speeds for the 0° direction are listed in Table 3. The speeds seen in each dual-PZT excitation case agree with speeds seen in the single-PZT excitation case.

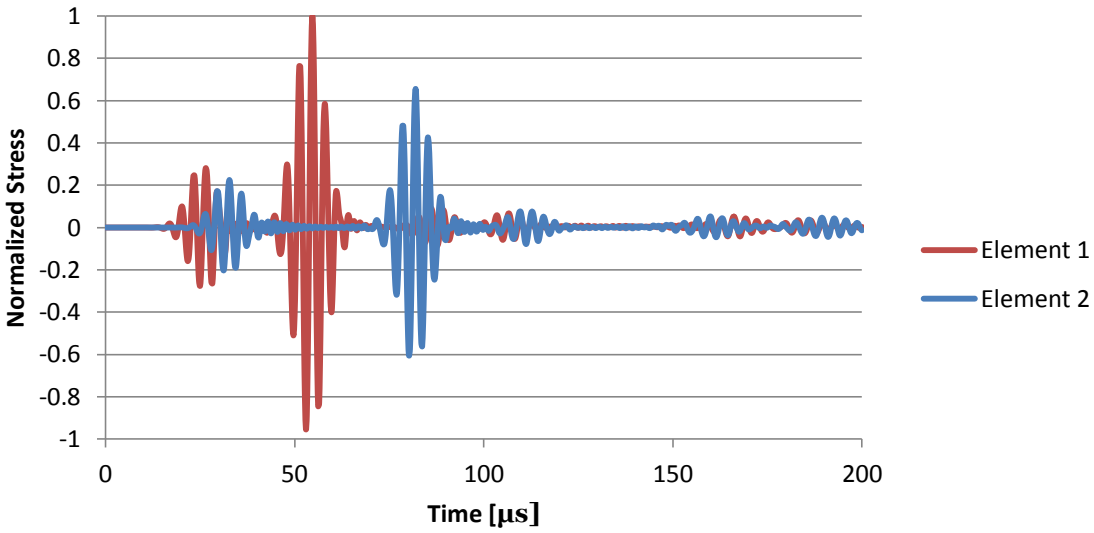

Figure 17. Numerical simulation single PZT excitation, *x*-stress.

Table 3

Calculated Group Velocity from Numerical Simulations in km/s

	Excitation Type		
Lamb Mode	Dual-PZT Symmetric	Dual-PZT Antisymmetric	Single-PZT
S_0	6.67	-	6.92
A_0	-	1.52	1.52

The numerical simulation was also able to provide full-field views of the propagating waves for each excitation case. Figures 18, 19, and 20 show the views of the top surface of the simulated plate at 46 μs for the symmetric, antisymmetric, and single-PZT excitations, respectively. The symmetric case has only the S_0 mode and the antisymmetric case has only the

A_0 mode. It is evident from the single-PZT excitation case that both modes are present, as the wider fringes account for the S_0 mode and the narrower fringes account for the A_0 mode.

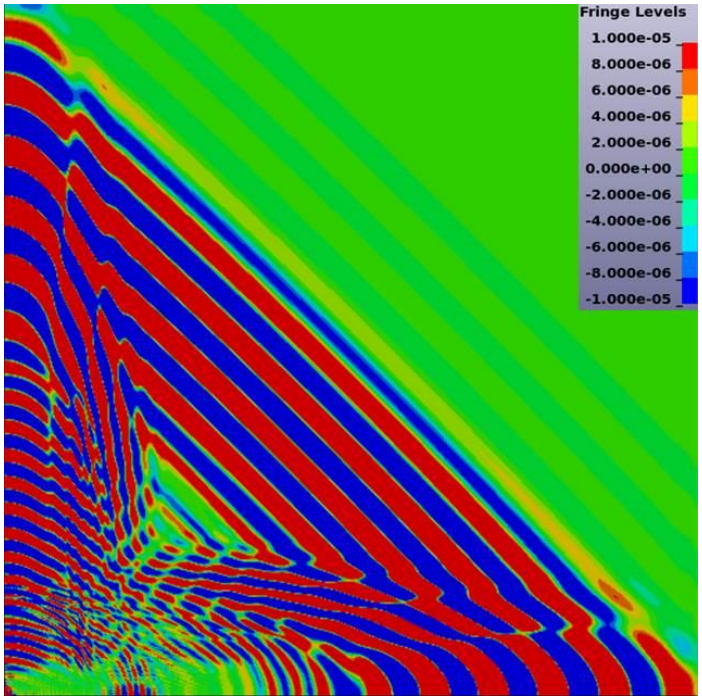

Figure 18. Simulated symmetric excitation full-field view

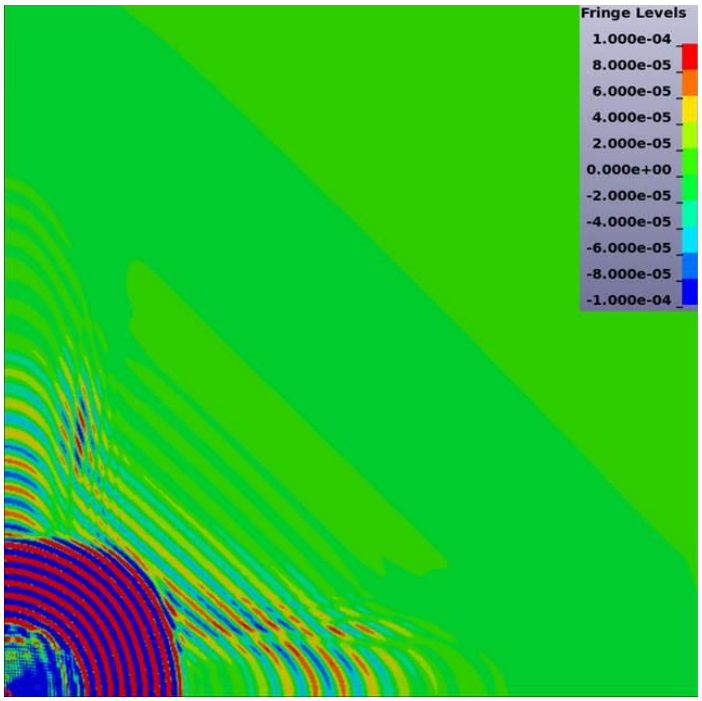

Figure 19. Simulated antisymmetric excitation full-field view.

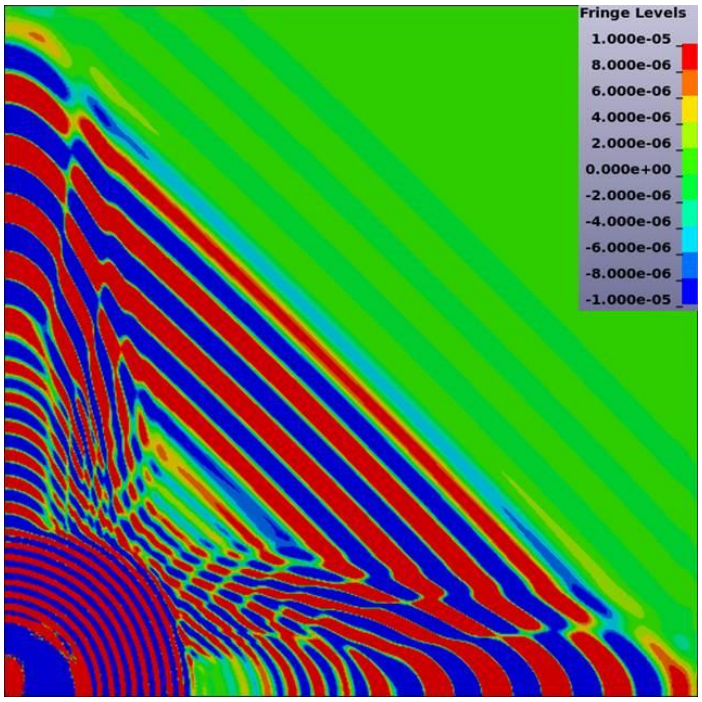

Figure 20. Simulated single-PZT excitation full-field view.

While the full-field views provided an idea of how the wave propagation appears, the waveforms were able to provide additional information, such as the group velocities calculated earlier. From the waveforms, the amplitude of the modes could be determined along each direction, as well. The amplitudes taken for each excitation case were determined by selecting nodes at the same distance for angles between 0° and 90° at 15° increments. Since attenuation was not modeled in the simulation, the reduction in amplitude for nodes at successive distances would not provide additional information about the nature of the wave propagation, other than the inherent geometric spreading. The data for the normalized amplitudes for each case and each mode is plotted in Figure 21. Little difference is seen between the amplitudes of the respective modes for the single-PZT excitation and the dual-PZT excitation. In fact, the *z*-displacement amplitudes taken for the symmetric case and the S_0 mode of the single-PZT case are completely coincident.

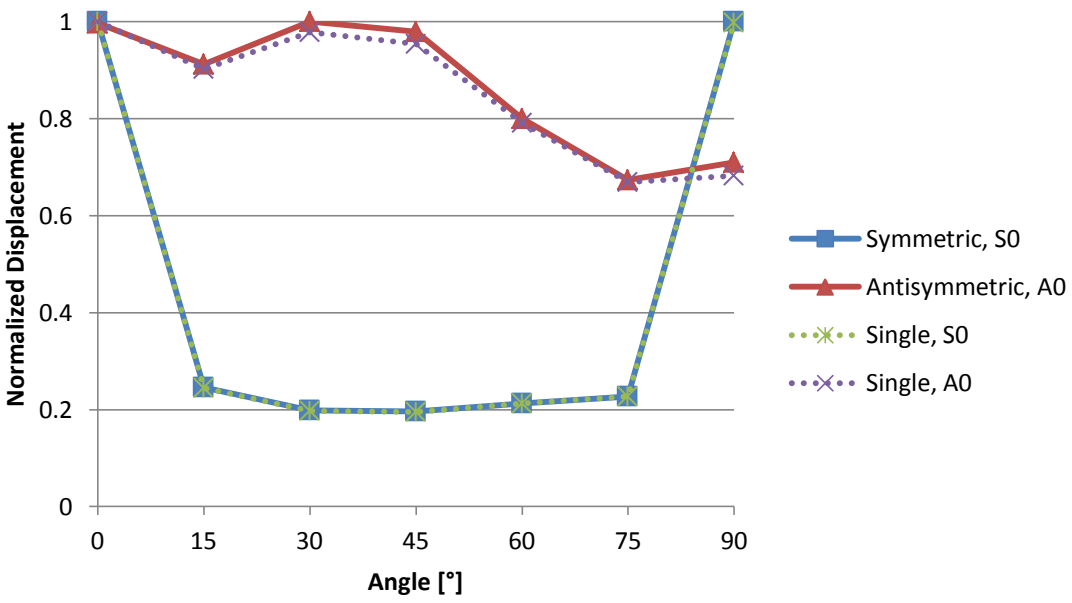

Figure 21. Amplitude comparison between the excitation cases for the simulation.

4.2 Experimental

4.2.1 Dual- vs. single-PZT excitation. A representative waveform captured on the oscilloscope for the dual-PZT symmetric excitation of the aluminum plate at 300 kHz is displayed in Figure 22. Similarly, a waveform taken from the excitation of the aluminum plate on the opposite side of the ultrasonic transducer can be seen in Figure 23. Waveforms similar to those in Figures 22 and 23 were captured for 200, 250, 300, 350, 400, 450, and 500 kHz. Waveforms past 500 kHz were not collected since higher frequencies give rise to multiple modes other than the fundamental Lamb modes. In fact, even at 500 kHz the A_0 mode could not be identified due to interference with higher wave modes. The waveforms captured were also for dual-PZT symmetric, dual-PZT antisymmetric, single-PZT same side as the transducer, and single-PZT opposite side of the transducer excitation. In total, twenty-eight waveforms were collected and analyzed.

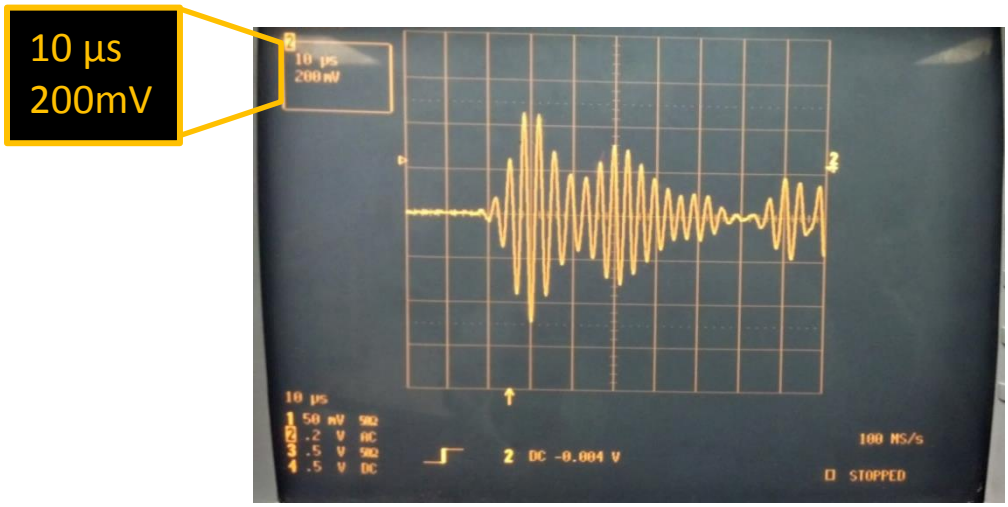

Figure 22. Oscilloscope display for dual-PZT symmetric excitation at 300 kHz.

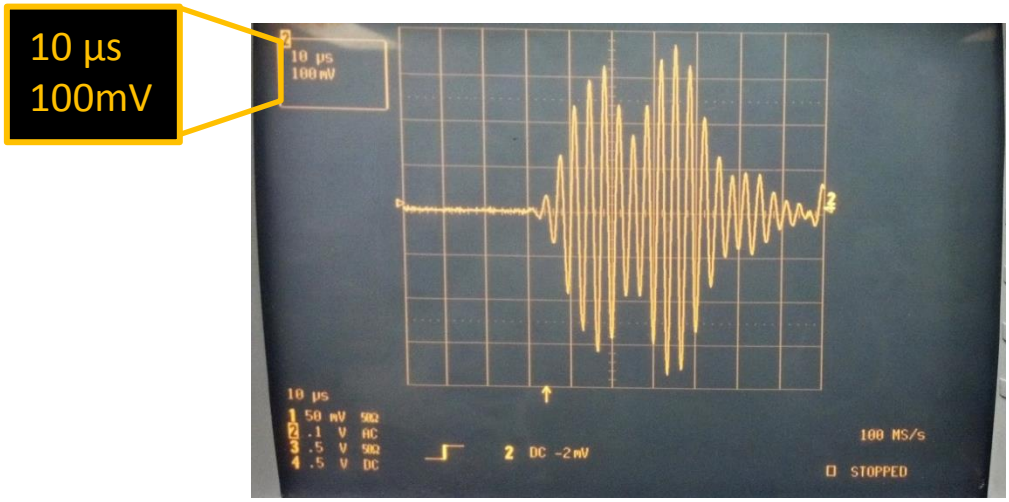

Figure 23. Oscilloscope display for single-PZT opposite side excitation at 300 kHz.

The waveforms were found to be similar in that the maxima of the S_0 and A_0 modes were equally spaced apart, roughly 20 µs for the 300 kHz case. The similarity seen between waveforms is consistent with the fact that phase velocities of a particular mode are the same along all directions in isotropic media. The differences arose in the amplitude of the S_0 and A_0 modes. (Note: the scale in Figure 22 is 200 mV/division while in Figure 23 the scale is only 100 mV/division.) Though symmetric excitation was used to improve the amplitude of the S_0 mode, the A_0 mode was still present to a lesser degree than the S_0 mode, as can be seen in Figure 22.

The same was true for antisymmetric excitation: the S_0 mode was still present to a lesser degree while the A_0 mode was amplified.

For each captured waveform, the amplitude of each mode was extracted by adding the maximum and minimum values of the respective mode (the total voltage between the peak and the trough). To determine how well the dual-PZT excitation method improved the amplitude of the desired mode, comparisons had to be made with the single-PZT excitation methods. Figures 24 and 25 show these comparisons for symmetric and antisymmetric excitation, respectively. For both cases, the generation of the desired mode was shown to have significant improvement with the dual-PZT excitation over both single-PZT excitation mechanisms up to 400 kHz. Both cases also exhibited a drastic drop in amplitude at 350 kHz, though the amplitudes of the antisymmetric excitation case remained above those of the single-PZT excitation cases, even at 450 kHz. However, for the symmetric excitation case at 450 and 500 kHz, the amplitude was seen to have decreased even below that of the single-PZT excitation on the opposite side of the ultrasonic transducer. These results were similar to those taken by Asamene (2013), though the drop in amplitude was first seen at 400 kHz in his research.

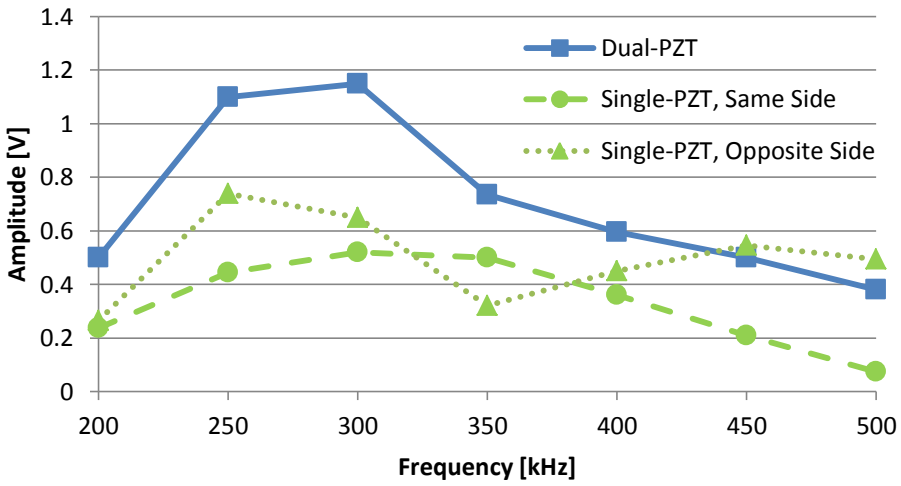

Figure 24. Amplitude variations for S_0 with symmetric and single-PZT excitation.

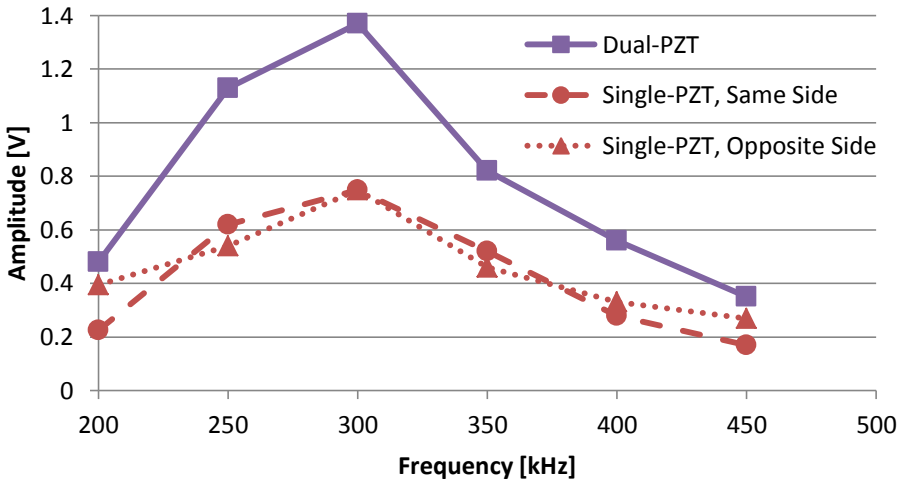

Figure 25. Amplitude variations for A_0 with antisymmetric and single-PZT excitation.

Due to the results of this aluminum plate test, the dual-PZT excitation method was selected to be applied to perform the remaining experiments on the composite laminate at 300 kHz. Since the amplitude found for each case at 300 kHz was nearly or more than doubled (percentage increases of at least 77% for symmetric excitation and 83% for antisymmetric excitation), much higher amplitude results could be acquired with the PSV for dual-PZT excitation at this frequency than for single-PZT excitation. The higher amplitude signals achieved would also have a higher, more desirable signal-to-noise ratio.

4.2.2 Identification of the fundamental Lamb modes. Since Lamb wave patterns in composite laminates were not readily available, the fundamental Lamb modes had to be identified from the extracted wavefield information. To confidently determine the location in time that each mode arrives, a test was performed. For this test, single excitation was imposed on each side of the composite panel with the bonded PZT wafer at the center of the panel, as in the single-PZT aluminum test experiment. The wavefields were extracted individually by the PSV, and in the post-processing phase of the PSV system, the scan data from a single point was selected for view. The scan data, out-of-plane displacement versus time, was exported to allow

for reconstruction and superposition of the two waveforms for Lamb wave mode identification purposes.

Scan data for single PZT excitation at 3 inches from the source along the 0° direction has been combined and is shown in Figure 26. The S_0 mode is identified as the first wave packet, as it travels much faster than the A_0 mode. The S_0 mode was also concurrent and had similar out-of-plane displacement magnitude. The time of arrival of the S_0 mode peak occurs at 31 μs at this distance and along this direction. The A_0 mode could be identified by the portion of the superposed waveforms that resulted in a 180° out-of-phase region. While the peak of the A_0 mode experienced a shift due to reflections from the top edge, the approximate time of arrival was selected from the higher amplitude response to be 83 μs at this distance and along this direction.

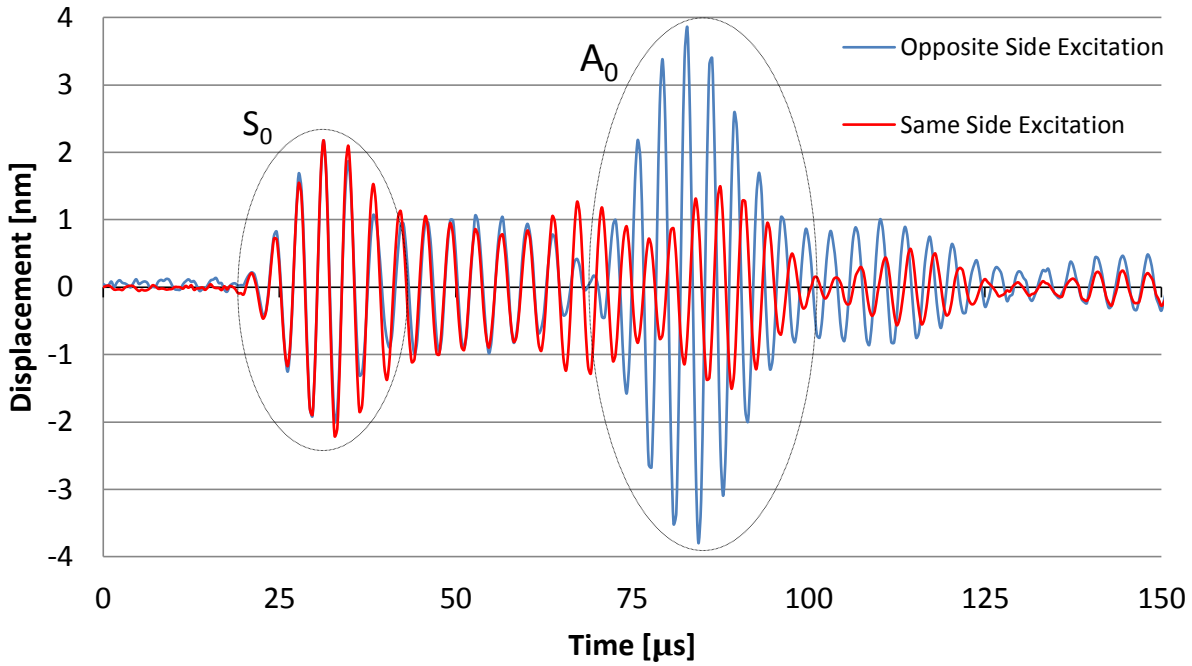

Figure 26. Scan data for identifying the fundamental Lamb wave modes.

From the time of arrival data extracted from the waveforms, group velocity for each of the modes along each direction could be computed. The difference in the time of arrival for each wave mode taken at different locations along the same direction was divided by distance between the two locations to determine group velocity. Table 4 gives the calculated group velocity values for the S_0 and A_0 modes and for each direction. These values were found to be consistent with past research conducted in this lab on a cross-ply composite laminate (Asamene, 2013).

Table 4

Calculated Group Velocity in km/s

	Angle (°)						
Lamb Mode	0	15	30	45	60	75	90
S_0	6.51	5.52	4.98	5.40	4.98	6.51	6.80
A_0	1.62	1.55	1.55	1.59	1.51	1.49	1.57

4.2.3 Amplitude vs. distance. The full-field representation of the Lamb waves propagating through the cross-ply CFRP laminate using a radial scan grid and symmetric excitation is presented in Figure 27. The maximum and minimum out-of-plane displacements have been scaled down from 20 nm to 2 nm to better view the smaller amplitude S_0 waves propagating far from the source. While the image taken from the radial scan grid is a full-field view, it is important to note that interpolations take place in the regions between the scan points.

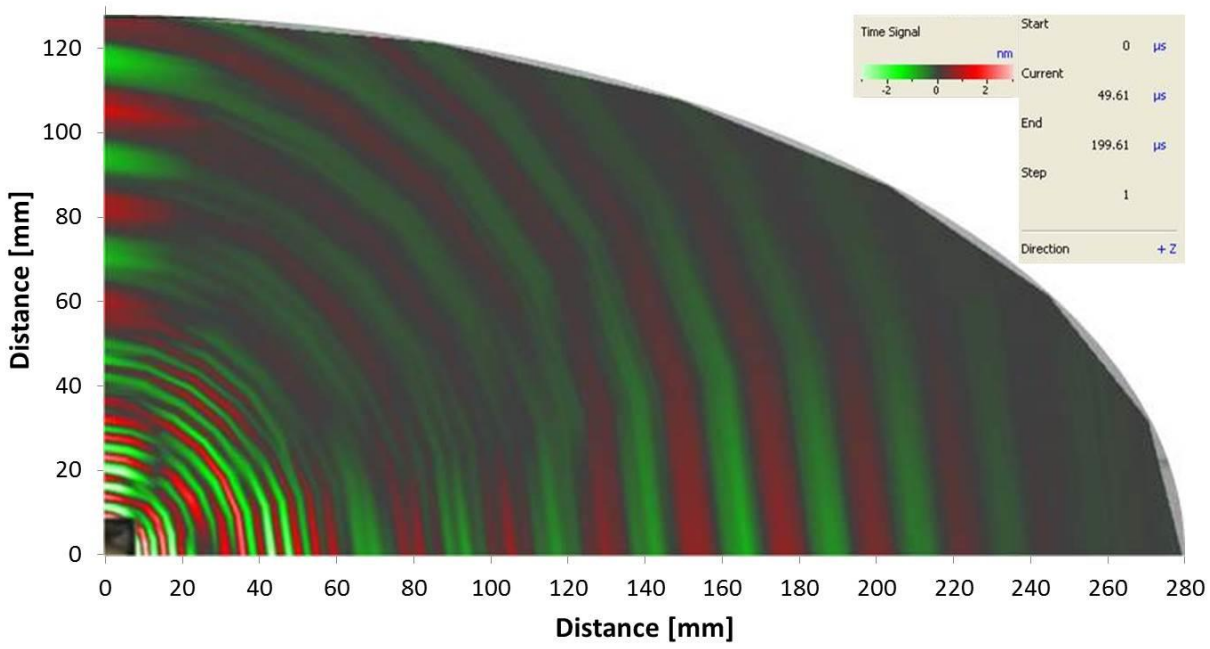

Figure 27. SLV results at 49.51µs for symmetric excitation.

At the time of the scan of 49.51 µs in Figure 27, the S_0 wavefields (wider fringes) have propagated much further than the A_0 wavefields (narrow fringes near the source at the origin), which is consistent with the large difference in the calculated group velocities. In order to verify the calculated group velocities with the full-field image, the leading portion of the input pulse that was at or very near zero, or delay time, had to be resolved to locate the actual time the first peak of the pulse deflected the plate. From the input pulse, the delay time was found to be 11 µs. Given this delay, the wave shown in Figure 27 actually propagated for only 38.51 µs. Using the calculated group velocities, the leading peak of the S_0 mode should be at 250.7 mm. Similarly for the A_0, the leading peak should be present at 62.7 mm. The full-field image clearly displays these fringes in red for positive out-of-plane displacement at these distances for the respective modes.

Had the image in Figure 27 not been scaled to exaggerate the out-of-plane displacement, it would have been very difficult to distinguish the S_0 fringes due to the attenuation of the wave

as it propagated throughout the scan area. In order to determine the degree to which the wave modes attenuated, the overall displacement amplitudes at discrete points on the wavefield were measured along each direction. For the symmetric excitation, the S_0 mode travelled well enough to be able to take measurements at 1 in (25.4 mm) increments along each direction. For the antisymmetric excitation, the amplitude of the A_0 mode was too low past a few inches to be able to distinguish between the propagating wave mode and the noise level. As a consequence, the measurements had to be taken at ½ in increments in order to develop an amplitude profile.

Due to the limitations of the geometry of the plate, reliable measurements without interference from immediate reflections could only be extracted at a distance of up to 11 in along the 0° direction and 5 in along the 90° direction. Intermediate directions varied between these lengths based on the dimensions of the scan grid. In addition, the measurements initially taken for the symmetric excitation case at 1 in for most directions (75° being the exception) were found to be unreliable as this distance is too close to the source to allow for sufficient separation of the wave modes. For this reason, the first point where the wave modes were clearly separated was selected for amplitude measurement. At half an inch for the antisymmetric mode, the placement of the PZT posed a problem as no information was able to be collected in this region for some directions. Again, the first point available was selected for measurement, with the distance change noted. Similar to the symmetric excitation case, the modes had not separated prior to 1 in, but given that the A_0 mode did not propagate far enough to allow for suitable separation, the measurements were taken, nonetheless. As with the waveforms from the oscilloscope for the aluminum plate experiment, the amplitude was taken to be the peak-to-trough difference. From these measurements, the displacement amplitude versus distance profiles were constructed and are presented in Figures 28 and 29 for the symmetric and antisymmetric excitation, respectively.

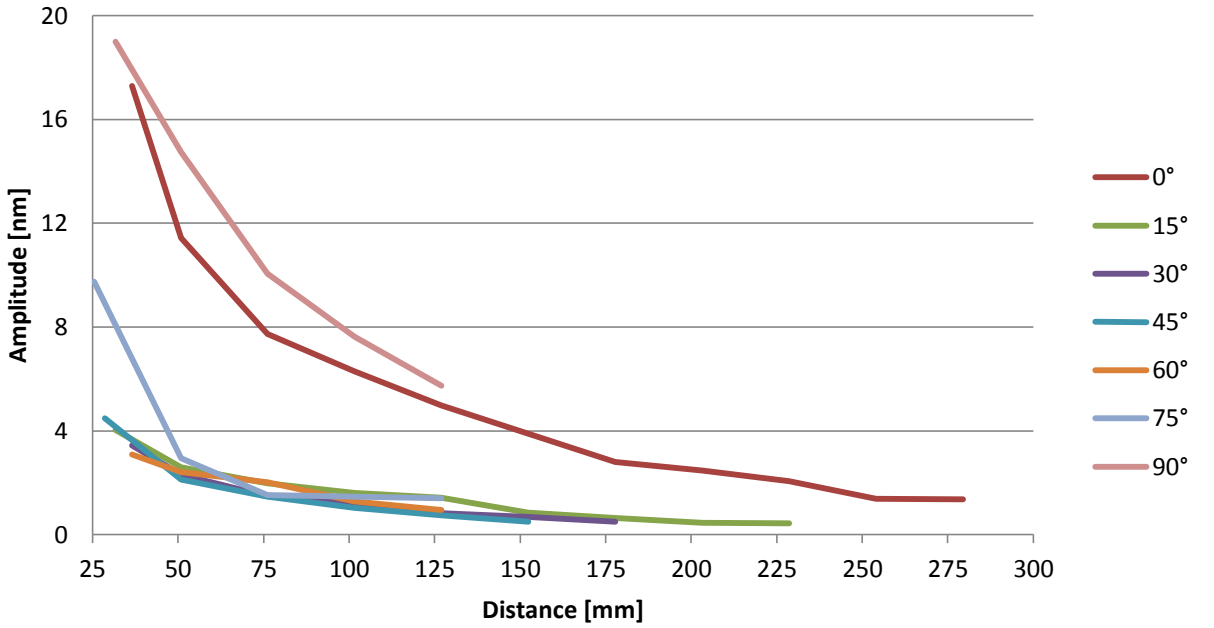

Figure 28. S_0 displacement amplitude profile.

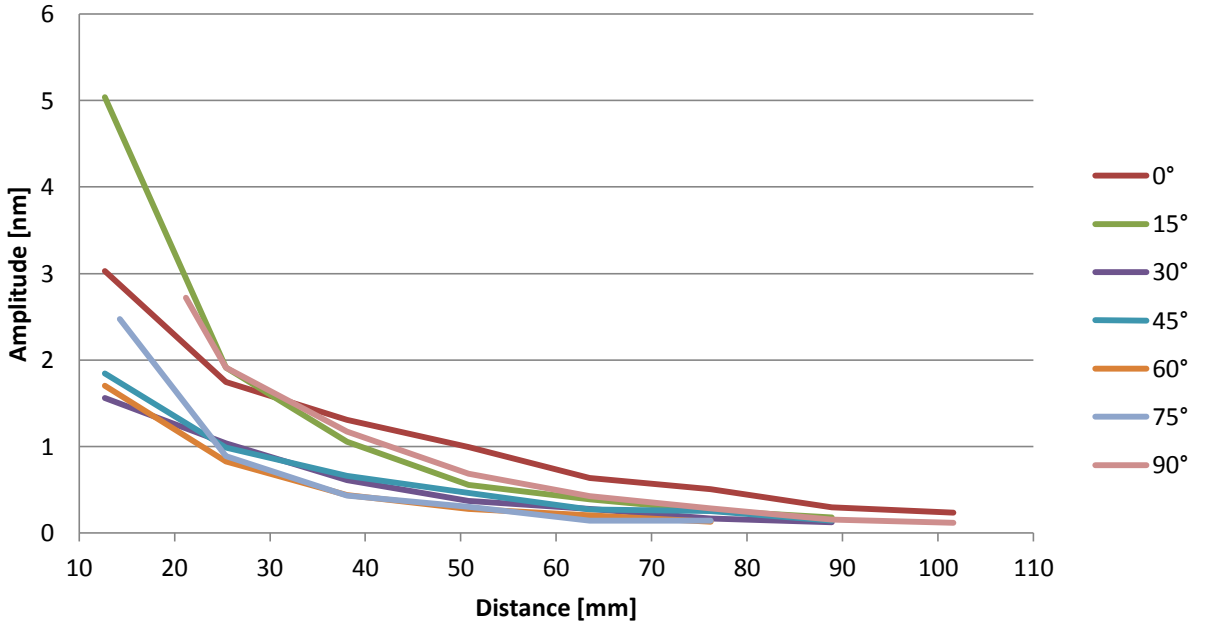

Figure 29. A_0 displacement amplitude profile.

From the above profiles, some observations can be made about each mode. For the S_0 mode, much higher amplitude signals were achieved along the fiber directions. The next highest

amplitudes were seen along the directions closest to the fiber directions, 15° and 75°. The remaining directions had very low amplitudes, less than 20% of those along the fiber direction, even in the vicinity of the source. For the A_0 mode, the amplitude was variable with propagation direction, with no particular direction exhibiting distinct characteristics. One reason for the lack of distinction could be that for the very low amplitude displacements measured, in many cases on the order of picometers, the A_0 results were obscured by noise even at the relatively short distance of 3 in.

The overall percentage decrease for each angle was also obtained from the amplitude data, and is shown for the S_0 mode in Figure 30 and the A_0 mode in Figure 31. For the S_0 mode, the highest initial percentage amplitude decrease occurred along the 75° angle with the 45° percentage decrease not much less. For the A_0 excitation, the most conclusive observation is that the 0° direction exhibited the least amount of amplitude reduction.

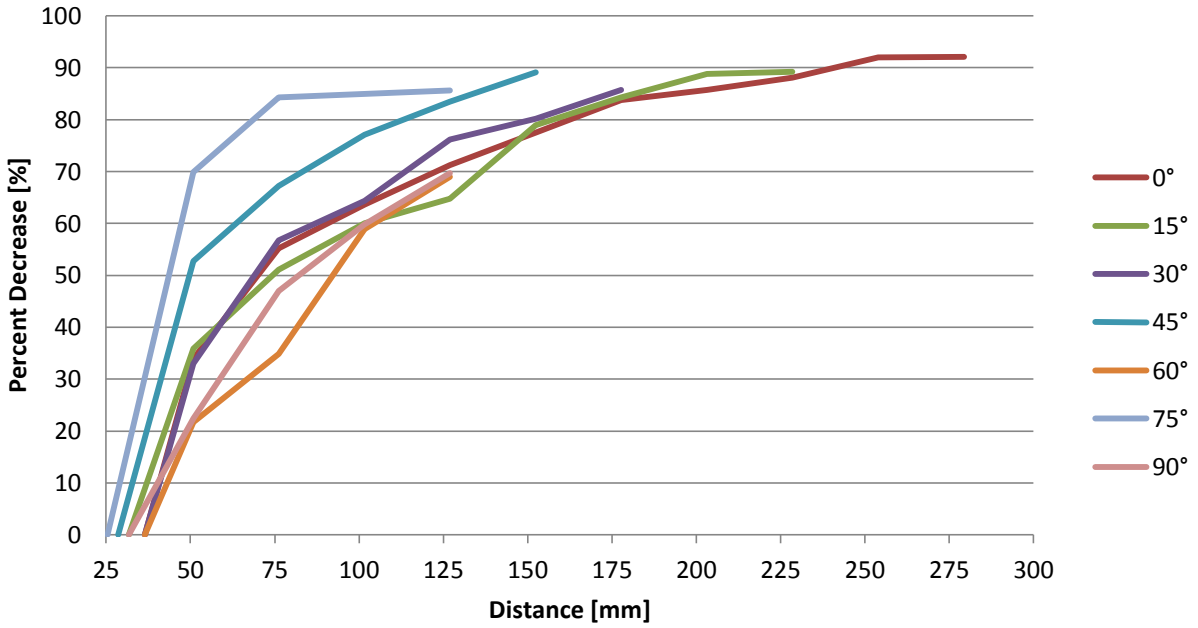

Figure 30. S_0 mode percentage decrease.

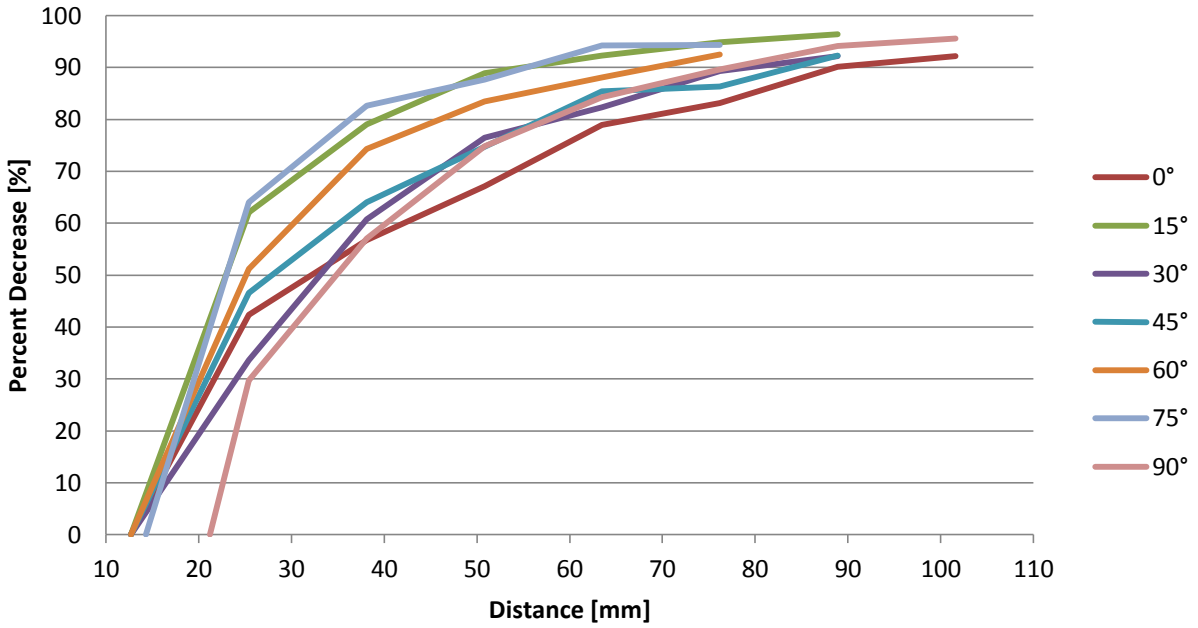

Figure 31. A_0 mode percentage decrease.

4.2.4 Attenuation coefficients. From the data collected about the displacement amplitude, attenuation coefficients could be calculated along each direction for each wave mode. A past study on attenuation measurements conducted by Luangvilai (2007) related the attenuation coefficient to the measured amplitude by the normalized magnitude spectrum, which is the measured time-domain signal normalized with the corresponding propagation distance, resulting in a unit-less magnitude. Tables 5 and 6 contain the normalized magnitude spectra for the respective wave modes for symmetric and antisymmetric excitation, respectively. Note that the first value in each column does not correspond exactly to 25.4 mm due to the limitations of the plate geometry mentioned in the previous section. The calculations conducted, however, did take into account the exact propagation distance to ensure accurate representation of the wave propagation. Also, for 75° at 101.6 mm, the measurement data was variable in the vicinity of the data point (possibly due to reflection interference), so no definitive value could be selected.

Table 5

Normalized Magnitude Spectra for Symmetric Excitation

	Angle (°)						
Distance (mm)	0	15	30	45	60	75	90
~25.4	20.73	4.51	4.12	4.75	3.70	9.75	21.23
50.8	13.48	3.27	2.72	2.82	2.85	4.16	18.64
76.2	11.18	3.06	2.15	2.40	2.90	2.66	15.59
101.6	10.49	2.88	2.04	1.94	2.12	-	13.64
127	9.27	2.84	1.53	1.56	1.78	3.13	11.49
152.4	7.96	1.86	1.40	1.13	-	-	-
177.8	6.20	1.50	1.09	-	-	-	-
203.2	5.83	1.15	-	-	-	-	-
228.6	5.17	1.17	-	-	-	-	-
254	3.66	-	-	-	-	-	-
279.4	3.79	-	-	-	-	-	-

Table 6

Normalized Magnitude Spectra for Antisymmetric Excitation

	Angle (°)						
Distance (mm)	0	15	30	45	60	75	90
~12.7	2.14	3.56	1.10	1.30	1.20	1.85	2.48
25.4	2.47	2.70	1.47	1.39	1.17	1.19	2.10
38.1	2.27	1.83	1.06	1.15	0.76	0.70	1.57
50.8	1.99	1.11	0.74	0.93	0.56	0.58	1.06
63.5	1.42	0.87	0.62	0.60	0.45	0.30	0.74
76.2	1.25	0.64	0.41	0.62	0.31	0.32	0.54
88.9	0.79	0.48	0.32	0.38	-	-	0.32
101.6	0.67	-	-	-	-	-	0.26

Once the normalized magnitude spectra were obtained, the attenuation coefficient could be determined by

$$\begin{Bmatrix} -\alpha \\ \ln|Q| \end{Bmatrix} = \begin{bmatrix} \sum_{i=1}^{N} x_i^2 & \sum_{i=1}^{N} x_i \\ \sum_{i=1}^{N} x_i & N \end{bmatrix}^{-1} \begin{Bmatrix} \sum_{i=1}^{N} x_i \ln|\bar{U}_i| \\ \sum_{i=1}^{N} \ln|\bar{U}_i| \end{Bmatrix}, \tag{6}$$

where $|\bar{U}_i|$ is the normalized magnitude spectrum, $|Q|$ is the source strength, x_i is the measured displacement amplitude taken at i, or the index of the measurement from 1 to N, with N being the number of measurements taken. The data was input into Matlab® to perform the summations and matrix multiplication and provide an attenuation coefficient for each wave mode along each direction. The resulting calculated attenuation coefficients are tabulated in Table 7.

Table 7

Calculated Attenuation Coefficients in Np/m

	Angle (°)						
Lamb Mode	0	15	30	45	60	75	90
S_0	6.39	6.95	8.25	10.46	7.50	10.08	6.37
A_0	14.96	28.16	19.11	16.83	22.21	29.78	28.43

As recognized previously, the 0° and 90° directions have considerably less attenuation for the S_0 mode. However, the 0° direction for the A_0 mode had the least attenuation while the 90° direction had an attenuation coefficient that was among the highest. This is most likely due to the fact that the measurements taken along the 90° direction were in close proximity to the high amplitude reflections from the top edge. The same may be said for the 75° direction, as well, which attenuated the most. Challenges were presented in being able to identify if a reflection was interfering, and whether constructive or destructive interference occurred was not able to be determined.

4.2.5 Aluminum vs. cross-ply composite laminate. The results captured from the dual-PZT excitation measurements on the cross-ply composite laminate were not consistent with the dual-PZT test on the aluminum plate. While the S0 mode was successfully enhanced by the symmetric excitation, the A_0 mode was dampened considerably by the antisymmetric excitation. The values obtained for A_0 for single-PZT excitation were at least six times as high as those obtained for the dual-PZT antisymmetric excitation at a distance of 76.2 mm. One potential explanation for the dampening seen is the layup of the composite structure. The layup of the cross-ply laminate used was symmetric, which lends itself easily to symmetric excitation about the midplane. Also, antisymmetric excitation could be impeded by the two similar plies along the midplane which would butt up against one another, allowing very little room for displacement. As such, antisymmetric excitation of symmetric laminates would neither yield strong enough signals nor favorable results for SHM applications.

4.2.6 Numerical simulation vs. experiment. The group velocities calculated for the simulated cross-ply laminate along the 0° direction in Table 3 are similar to the group velocities calculated from experiments in Table 4. While the amplitudes are not able to be compared due to the lack of attenuation in the simulation, the full-field wavefields captured can be. Figure 32 shows the full-field view of the cross-ply laminate image captured with the SLV at 46 μs using a rectangular grid. The SLV image is comparable to the simulated wavefield for single-PZT excitation in Figure 20. These wavefield images are also reminiscent of those captured by Ruzzene et al. (2004) during their investigation of ultrasonic waves in elastic plates using laser vibrometry.

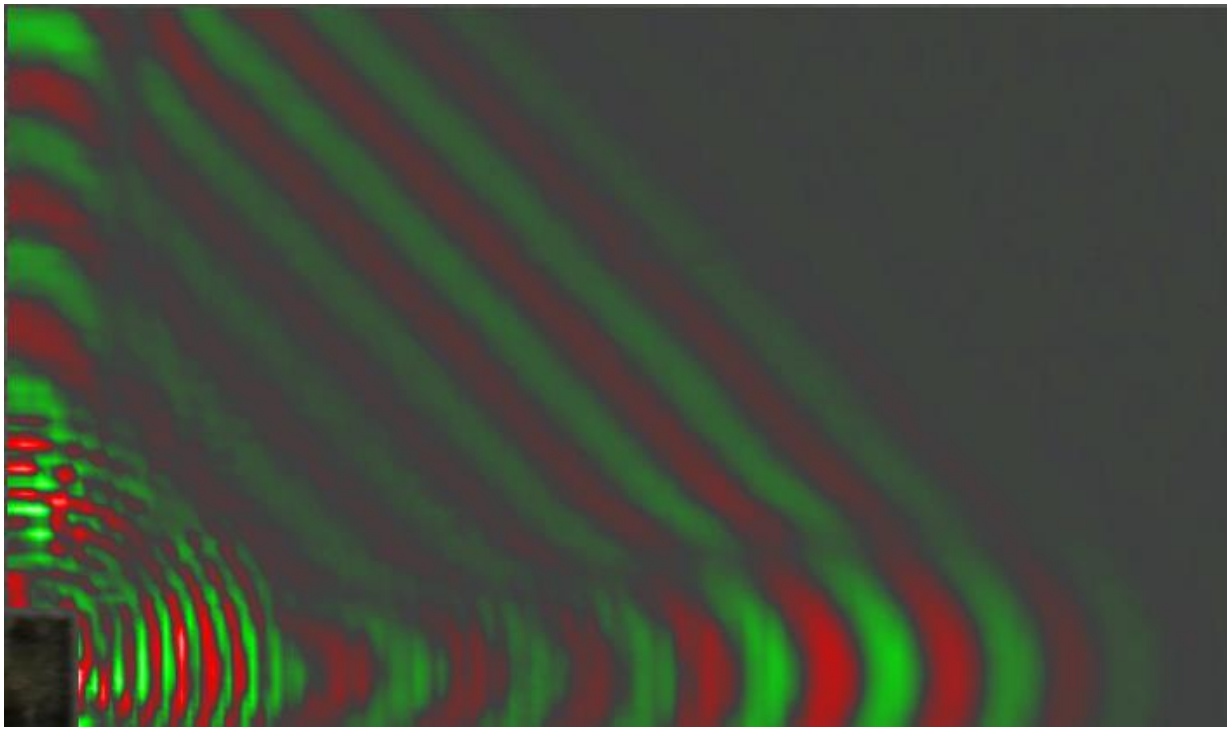

Figure 32. Full-field view of the cross-ply laminate, captured with the SLV.

CHAPTER 5

Discussion and Future Research

The amplitude, velocity, and attenuation were able to be characterized in the experiments over the area of the cross-ply laminate at 15° intervals. The highest amplitudes and speeds of the S_0 mode occurred along the fiber directions, with the least amount of attenuation occurring along these directions, as well. The A_0 mode showed little to no directionality for the amplitude, velocity and attenuation, however.

The experimental results found for the group velocity matched those found with the numerical simulation, proving the presence of only the fundamental Lamb wave modes during the SLV experimentation. Though attenuation was not able to be modeled in the simulation, geometric spreading was exhibited, seen in the reduction of the amplitude of the wave modes as they travelled along the plate. The simulated model and the experimental SLV wavefields were able to provide full-field views that showed similar patterns of the wave propagation.

The inability to determine the true displacement amplitude due to reflection interference introduced considerable, unquantifiable error into some of the presented experimental data. For future experimentation, to validate these results, a larger plate will be necessary. In addition, the A_0 mode was diminished by the antisymmetric excitation in the symmetric, cross-ply laminate, though the amplitude was amplified significantly in the aluminum plate. More investigation into the proper PZT width to A_0 wavelength ratio could potentially rectify the discrepancy in the amplitude.

The scanning laser vibrometry technique used in the present research offered a quick method of capturing a great amount of information about the wave propagation over a large area. The same information captured in this research by other methods could only be obtained at

discrete points using an ultrasonic transducer or PZT sensors, with extensive equipment setup time. The full-field views of the propagating waves provided additional information for verification that other ultrasonic NDE tests are not capable of readily providing. Other future experiments could employ the SLV for critical damage detection. The damage detection that was performed previously in much of the literature reviewed for the present research did not utilize scanning laser vibrometry, so much work can be done to improve the methods.

References

Adams, T. (2007, March). Acoustic verification of composites. *Advanced Materials & Processes*, *165*(3), 41-43. Retrieved from http://www.sonoscan.com/images/AcousticVerificationofComposites-AMPMarch2007.pdf

Alers, G. (1991). Methods for velocity and attenuation measurement. In A. S. Birks, R. E. Green, Jr. & P. McIntire (Eds.), *Nondestructive Testing Handbook* (2nd ed., Vol. 7, pp. 365-381). Albuqurque, NM: American Society for Nondestructive Testing.

Asamene, K. M. (2013). *Monitoring damage initiation and growth in composite structures by acoustic emission method*. (Unpublished doctoral dissertation).

Attenuation of sound waves. (2013, September 19). Retrieved from http://www.ndt-ed.org/EducationResources/CommunityCollege/Ultrasonics/Physics/attenuation.htm

Barbero, E. (2008). *Finite element analysis of composite materials*. (p. 68). Boca Raton, FL: CRC Press.

Carrara, M., & Ruzzene, M. (2013). *Numerical and experimental analysis of guided waves propagation in composite plates*. In *Proc. SPIE 8695* (pp. 86950W1-15). doi: 10.1117/12.2009866

Daniel, I., & Ishai, O. (2005). *Engineering mechanics of composite materials*. (2nd ed., pp. 9-10). New York, NY: Oxford University Press.

Diamanti, K., Soutis, C., & Hodgkinson, J. (2007). Piezoelectric transducer arrangement for the inspection of large composite structures. Composites Part A: Applied science and manufacturing, 38, 1121-1130. Retrieved from http://www.sciencedirect.com/science/article/pii/S1359835X06001941

Díaz-Valdés, H., & Soutis, C. (2002). Real-time nondestructive evaluation of fiber composite laminates using low-frequency lamb waves. *J. Acoust. Soc. Am., 111*(5), 2026-2033. doi: 10.1121/1.1466870

Giurgiutiu, V. (2005). Tuned lamb wave excitation and detection with piezoelectric wafer active sensors for structural health monitoring. *Journal of Intelligent Material Systems and Structures, 16,* 291-305. doi: 10.1177/1045389X05050106

Green, R. (1991). Introduction to Ultrasonic Testing. In A. S. Birks, R. E. Green, Jr. & P. McIntire (Eds.), *Nondestructive Testing Handbook* (2nd ed., Vol. 7, pp. 1-32). Albuqurque, NM: American Society for Nondestructive Testing.

Guo, N., & Cawley, P. (1993). The interaction of lamb waves with delaminations in composite laminates. *The Journal of the Acoustical Society of America, 94,* 2240-2246. doi: 10.1121/1.407495

Holford, K. M., & Lark, R. J. (2005). Acoustic emission testing of bridges. In G. Fu (Ed.), *Inspection and monitoring techniques for bridges and structures* (1 ed.). Retrieved from http://library.ncat.edu/search~S1?/.b1785583/.b1785583/1,1,1,B/l856~b1785583&FF=&1,0,,1,0

Johansmann, M., Siegmund, G., & Pineda, M. (2005).*Targeting the limits of laser Doppler vibrometry*. In *Proceedings of the International Disk Drive Equipment and Materials Association* (pp. 1-12). Retrieved from http://www.polytec.com/fileadmin/user_uploads/Applications/Data_Storage/Documents/LM_TP_Idema_JP_2005_E.pdf

Kessler, S., Spearing, S., & Soutis, C. (2001). *Optimization of lamb wave methods for damage detection in composite materials*. In *Proceedings of the 3rd International Workshop on Structural Health Monitoring*. Retrieved from http://www.metisdesign.com/docs/papers/SHM01.pdf

Luangvilai, K. (2007). *Attenuation of ultrasonic lamb waves with applications to material characterization and condition monitoring*. (Unpublished doctoral dissertation) Retrieved from https://smartech.gatech.edu/bitstream/handle/1853/16167/luangvilai_kritsakorn_200708_phd.pdf?sequence=1

Modes of sound wave propagation. (2013, September 19). Retrieved from http://www.ndt-ed.org/EducationResources/CommunityCollege/Ultrasonics/Physics/modepropagation.htm

Neumann, M., Hennings, B., & Lammering, R. (2012). Identification and avoidance of systematic measurement errors in lamb wave observation with one-dimensional scanning laser vibrometry. *Strain: An International Journal for Experimental Mechanics*, *49*(2), 95-101. doi: 10.1111/str.12015

Pai, F. (2007). *Highly flexible structures: Modeling, computation, and experimentation*. (pp. 27-31). Reston, VA: American Institute of Aeronautics and Astronautics, Inc.

Piezoelectric transducers. (2013, September 19). Retrieved from http://www.ndt-ed.org/EducationResources/CommunityCollege/Ultrasonics/EquipmentTrans/piezotransducers.htm

Polytec Scanning Vibrometer Manual, MAN-PSV-From Vers. 5.1-E2/01-9712.

PreSys™ Manual. Retrieved from http://mirror.eta.com/Software/Inventium/PreSys/Inventium_PreSys_2010_Quick_Start_Guide.pdf

Raghavan, A., & Cesnik, C. (2007). Review of guided-wave structural health monitoring. *The Shock and Vibration Digest*, *39*(2), 91-114. doi: 10.1177/0583102406075428

Rose, J. (1999). *Ultrasonic waves in solid media*. (pp. 101-103). Cambridge, UK: Cambridge University Press.

Ruzzene, M., Jeong, S., Michaels, T., Michaels, J., & Mi, B. (2004). *Simulation and measurement of ultrasonic waves in elastic plates using laser vibrometry*. In Thompson, D. O., Chimenti, D. E. (Eds.), *AIP Conference Proceedings* (pp. 172-179). doi: 10.1063/1.1916675

Sierakowski, R., & Chaturvedi, S. (1997). *Dynamic loading and characterization of fiber-reinforced composites*. (pp. 135-162). New York, NY: John Wiley & Sons, Inc.

Su, Z., & Ye, L. (2004). Selective generation of lamb wave modes and their propagation characteristics in defective composite laminates. *Journal of Materials: Design and Applications*, *218*(2), 95-110. doi: 10.1177/146442070421800204

Wang, L., & Yuan, F. G. (2007). Group velocity and characteristic wave curves of lamb waves in composites: Modeling and experiments. *Composites Science and Technology*, *67*(7-8), 1370-1384. Retrieved from http://www.sciencedirect.com/science/article/pii/S0266353806003630

Yang, C., Ye, L., Su, Z., & Bannister, M. (2006). Some aspects of numerical simulation for lamb wave propagation in composite laminates. *Composite Structures*, *75*(1-4), 267-275. doi: 10.1016/j.compstruct.2006.04.034